Aalto University
School of Chemical
Technology

School of Chemical Technology

Degree Programme of Chemical Technology

Kehinde Adewunmi Mustapha

Utilisation of microplant and reactive distillation for the production of 2-methoxy-2,4,4-trimethylpentane

Master's thesis for the degree of Master of Science in Technology

Espoo, 22 January, 2014.

Supervisor Professor Ville Alopaeus

Instructors D.Sc. Petri Uusi-Kyyny

M.Sc. Saeed Mardani

Aalto University
School of Chemical
Technology

Aalto University, P.O. BOX 11000, 00076 AALTO
www.aalto.fi

Abstract of master's thesis

Author: Kehinde Adewunmi Mustapha	
Title of thesis: Utilisation of micro-plant and reactive distillation for the production of 2-methoxy-2,4,4-trimethylpentane	
Department: Chemical engineering	
Professorship: Chemical engineering	**Code of professorship:** Ke-42
Thesis supervisor: Professor Ville Alopaeus	
Thesis instructors: D.Sc. Petri Uusi-Kyyny M.Sc. Saeed Mardani	
Date: 22.01.2014 **Number of pages:** 78 **Language:** English	

The micro-plant and reactive distillation concepts have been researched in this thesis. The aim of the project is to invent a technique for the production of pure 2-methoxy-2,4,4-trimethylpentane (TOME). After the production, physical property of interest of the chemical compound would be determined.

The first phase of this project relates to the production of TOME with the micro-plant constructed by Aalto University chemical engineering research group. In the second section, TOME was manufactured with reactive distillation principle. These two mechanisms were later compared, specifically for TOME production.

Special interest has been focused towards 2-methoxy-2,4,4-trimethylpentane for over a decade. 2-methoxy-2,4,4-trimethylpentane has been recognised as one of the few chemical compounds that could be utilised as fuel additive (fuel oxygenate) in gasoline pool. However, production of the pure chemical is very demanding.

In this thesis, all the obstacles encountered during production of this fuel oxygenate would be revealed. A range of separation principles have been implemented for the realisation of pure TOME. The time available for this project is very limited, notwithstanding density measurement of 2-methoxy-2,4,4-trimethylpentane and 2,4,4-trimethyl-1-pentene were conducted. The density measurement of these chemical compounds was accomplished at varying temperatures and compared with literature values.

Keywords: Micro-plant, reactive distillation, etherification, dimerisation, 2-methoxy-2,4,4-trimethylpentane, fuel oxygenate.

PREFACE

This thesis was conducted for Aalto University (formerly Helsinki University of Technology) chemical engineering research group from May to December, 2013. It was a part of the micro-plant project and the incorporation of reactive distillation technique.

Profound gratitude goes to Almighty God, my parents and siblings for the successful completion of this project. Their support over the years is really appreciated. I am very grateful to my supervisor, Professor Ville Alopaeus, for giving me the opportunity to be part of the research group of Aalto chemical engineering department.

I am deeply indebted to my instructor, Dr. Petri Uusi-Kyyny, for his proper guidance throughout the whole period of this project. He was very helpful in the provision of materials (journals) and invaluable advice for this thesis. I thank my second instructor and co-worker on this project, M.Sc. Saeed Mardani. The micro-plant and reactive distillation runs were jointly executed by both of us under the stewardship of Petri.

I am grateful to Dr. Juha Pekka-Pokki for his contribution and guidance in the reactive distillation runs. Everyone in the department that has contributed in one way or the other is also acknowledged. Generally, the working condition has been conducive. More so, the laboratory safety rules and obligations have been duly observed throughout the execution of this project.

Contents

NOMENCLATURE

Symbols

a	Activity
A	Area
B	Second coefficient of the virial equation
b	Parameter of the cubic equation of state
C	Third coefficient of the virial equation of state
D	Fourth coefficient of the virial equation of state
f	fugacity
F	Response factor
G	Gibbs free energy
M	Molar mass
P	Pressure
T	Temperature
R	Gas constant
x	Liquid phase molar fraction
y	Vapour phase molar fraction
Z	Compressibility factor

Greek notations

α	Temperature dependent alpha function
β	Temperature dependent beta function
γ	Liquid activity coefficient
ρ	Density
μ	Chemical potential
∅	Fugacity coefficient
$\bar{g}_i$	Partial molar Gibbs energy
ϕ	Phi

Superscripts and subscripts

ex	Excess
IM	Ideal mixture
L	Liquid phase
V	Vapour phase
^{0}	Standard state
i	Component
m	molar
vap	Vapour
lit	Literature
meas	Measured

Mathematical notations

Σ	Summation
∫	Integral
d	Derivative
In	Natural logarithm
exp	exponential

Abbreviations and Acronyms

DME	Dimethyl ether
EFOA	The European fuel oxygenates association
EOS	Equation of state
ETBE	Ethyl tert-butyl ether
FID	Flame indicator detector
GC	Gas chromatography
KF	Karl Fischer
LLE	Liquid-liquid equilibrium
MeOH	Methanol
MTBE	Methyl tert-butyl ether
POY	Poynting correction
RD	Reactive distillation
TAEE	Tert-amyl ethyl ether (2-ethoxy-2-methylpropane)
TAME	Tert-amyl methyl ether (2-methoxy-2-methylbutane)
TMP-1	2,4,4-trimethyl-1-pentene
TMP-2	2,4,4-trimethyl-2-pentene
VLE	Vapour-liquid equilibrium

1. Introduction

One of the most notable obstacles in the development of a novel process is the high cost of operation and the restriction to time frames reserved for developmental processes. Experimental investigations need be specifically target-oriented. Most especially when expensive hazardous reacting species are involved. If pilot plant operation is employed, this even contributes to the overall costs. This is as a consequence of chemical and labour costs, experiment time and safety of the process (Müller, 2013). One approach to overcome these problems is the implementation of micro-plants.

The potential benefit of micro-plant for accelerating process design and development complements the operations mini-plant has had for the past two decades. The cost of production of this plant can be quite moderate. The process configuration can be adjusted immediately. More so, the hold-up in this system is very low, improving the safety of the process. Consequently, the process requires less supervision, which directly results into reduced labour costs. The small hold-up in the process distinctly minimises chemical costs, particularly if extensive production has not been initiated (Sundberg et al., 2009). In Adeosun and Lawal et al. (2009 and 2010), asides the process and environmental safety potentials possessed by micro-plants, they also have the capacity to increase the yields.

According to Robbins (1979), Gress (1979) and Maeir (1990), micro-plants operate on laboratory-scale mechanism, possessing various complexities in form of essential unit operations and recycles of the process. Wörz (1995) proposed that the accumulative residence time for the recycles has to be lower than 24 h. Micro-distillation columns are important to effectively actualise the maximum capacity of the micro-plant units. Hold-up in micro-distillation is significantly lower than that experienced with mini-plant operations. In spite of the potentials of these units, very few endeavours have been conducted to upgrade this equipment (Sundberg et al., 2009).

On the other hand, reactive distillation (RD) is a specially designed apparatus used to improve the conversion of chemical products which might have been inhibited by reaction equilibrium. This could be accomplished by constantly withdrawing the product from the reaction zone. RD also has the economic potential of reducing overall investment and operating costs (Krishna, 2002).

The goal of this thesis is to device a technique for the production of 2-methoxy-2,4,4-trimethyl-1-pentane (TOME). In order to accomplish this target, the micro-plant developed by Aalto University chemical engineering research group was utilised. Afterwards, reactive distillation was also implemented for the production of TOME. The effectiveness of these two processes, particularly for TOME production, was then evaluated. Mixture of methanol and diisobutylene (primarily 2,4,4-trimethyl-1-pentene and 2,4,4-trimethyl-2-pentene) were introduced as the feed.

2. Micro-plant

The relationship of fluid dynamics, actual separation behavior and thermodynamics in real applications are not well established on laboratory-scale measurements. Hence, it is pertinent to bridge the gap between results of laboratory-scale measurements and the actual industrial operations. This necessitates the implementation of micro-plant for this purpose, built parallel to lab-scale research. The essential of micro-plant applications is to facilitate investigations regarding the impacts of catalysts effectiveness, accumulation of by-products, stability and catalyst loss during long time operations, controllability of reaction and the influence of recycles. With the accomplishment of this valuable information, the relevant measure towards industrial application will be accessible (Müller, 2013).

2.1 Micro-process technology

Micro-structured components in process engineering discipline have attained great popularity in pharmaceutical, chemical and life science (Hessel, 2004). Miniaturised reactors, distillation columns, mixers and heat exchangers can be constructed in a model measured in millimeters and incorporated with micro-scaled pores. The number of physical and chemical reactions employing micro-structured reactors, mixers, heat exchangers and micro-engineering applications is on the rise. The automotive, chemical and environmental industries are the major users. All these occur under inherently safe and highly selective conditions (Müller, 2005). Miniaturised devices have the ability to operate continuously and are highly automated. They are flexible equipment that screens rapidly at low material input. They can be easily manipulated from laboratory to production scale of operation (Ehrfeld, 1996).

The problem associated with micro-process technology is however the price of obtaining a single unit. The parts used to assemble a micro-plant are rather too exorbitant. Another major setback is incompatibility issues

experienced with devices from various manufacturers. Many suppliers are unable to provide a complete range of devices required for unit operations. The use of parts developed by different suppliers has not been successful in some instances (Müller, 2005).

'Modular micro-process engineering' was established in year 2000. The objective of this platform was to establish a notion for the establishment of a consistent standard and modular procedure to micro-process technology. This will help counteract the aforementioned downsides (incompatibility problems) and provide a cost-efficient result. There were about 45 research institutes, industrial users and suppliers as at year 2004. A manufacturer spanning building-set consisting of compatible micro-process components was also created (Müller, 2005).

2.2 Micro-plant in Aalto VLE laboratory

The micro-plant by Aalto chemical engineering research group was constructed for research on the micro-plant concept for process development. The main operational parts of the current setup are a tubular reactor and a distillation column. The reactor and distillation units are supplemented with devices such as pumps, tubes, temperature control units, flow meters, valves, gas chromatography and heat exchangers. The maximum capacity of the reactor is 79 cm^3.

For TOME production, the feed in a 0.50 dm^3 Schott Duran reagent bottle is usually introduced into the reactor via the pump demonstrated below in Figure 1. The feed is introduced into the reactor in batches owing to the small size of the reactor with the aid of the pump controller and valves. The product from the reactor is conveyed to the gas chromatography unit where analysis occurs. The remaining product is later transferred to another reagent bottle. The composition of the product is composed of TOME, unreacted methanol, diisobutylene, a compound reported as alcohol, dimethyl ether, a host of other impurities and water produced from the side reaction in this process.

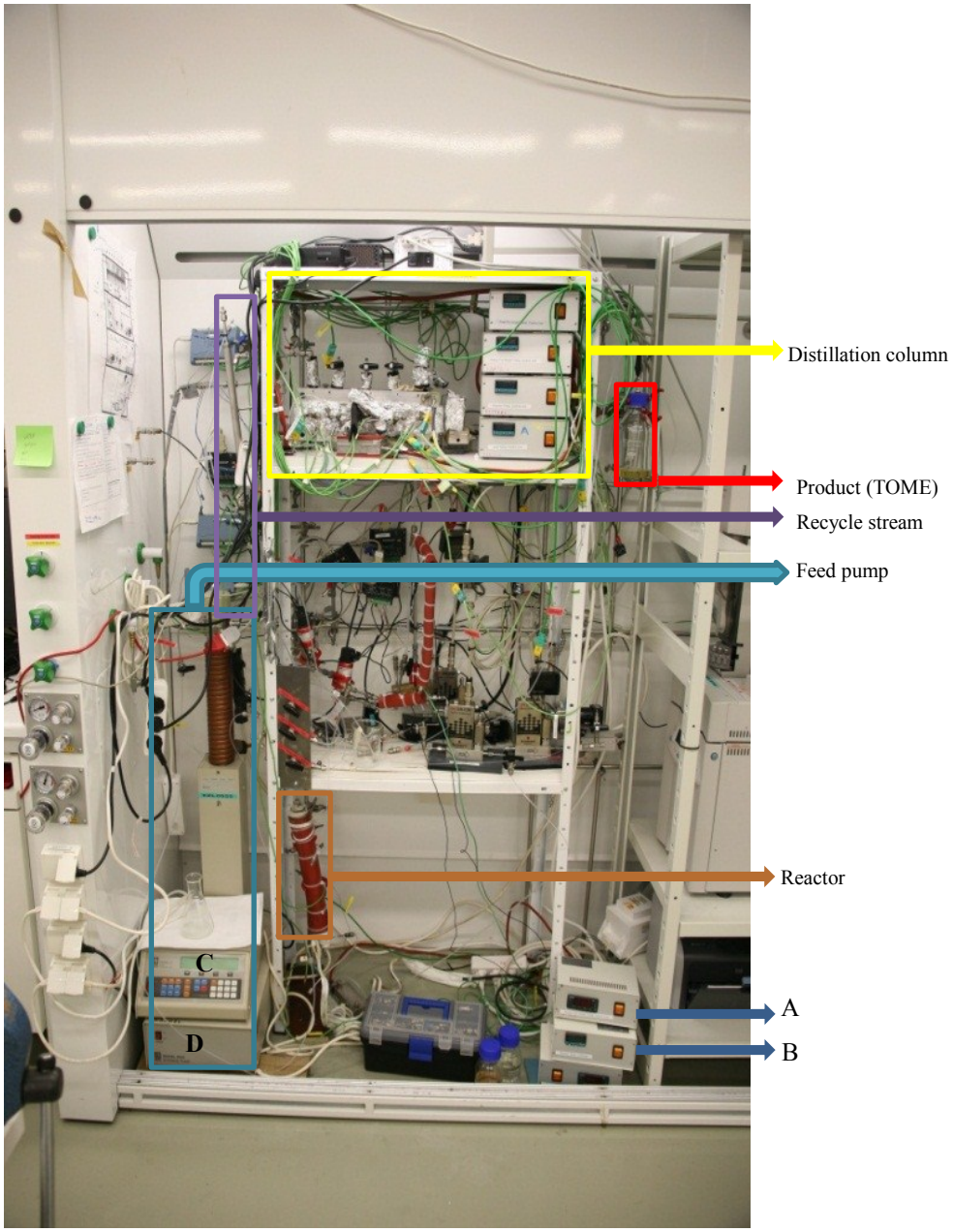

Figure 1: Micro-plant constructed by chemical engineering research group, Aalto University. A; reactor pre-heater temperature controller unit, B; reactor temperature controller, C; ISCO SFX 200 controller, D; model 500D syringe pump.

3. Reactive distillation

Reactive distillation (RD) involves the integration of both chemical reaction and phase separation (distillation) in a single column. In some systems, they are more economical than the combination of traditional reactor and separation, with or without recycles, specifically for reversible reactions in which conversion in a conventional reactor is inhibited by chemical equilibrium constraints. The operating temperature has to be favorable for both reaction and separation since both processes occur simultaneously in a column at a specific pressure. Therefore, this condition then limits the implementation of RD for systems in which mutual temperature exists for both reaction and vapour-liquid equilibrium (Luyben, 2006).

However, RD has gained remarkable recognition from industry and academia due to the numerous benefits it possesses over conventional processes having sequential arrangement of a reactor and distillation. The application of reactive distillation can be specifically beneficial for reaction systems in which maximum conversion is hindered by chemical equilibrium (Doherty and Buzad, 1992; Malone and Doherty, 2000).

The figure below is a demonstration of a reactive distillation column. Two feeds (methanol and diisobutylene) were introduced into the column. The methanol is concentrated at the distillate section, being the lighter component with some traces of unreacted reactant. At the bottom product, the ether formed remains with the unreacted reactants.

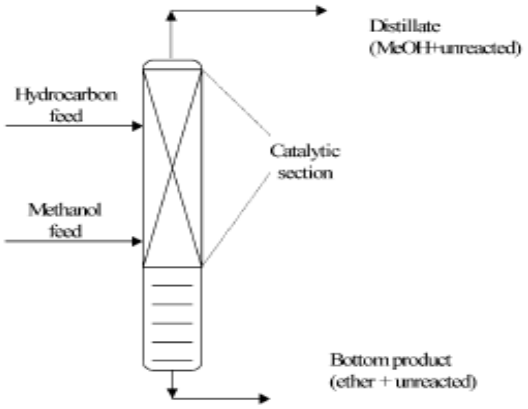

Figure 2: Diagram showing the process configuration of reactive distillation (Rihko-Struckmann et al., 2002).

In reactive distillation, tray hold-up or amount of catalyst has immense impact on product composition, conversion and column composition profiles. So, tray hold-up should also be considered along with normal design parameters such as number of trays, reflux ratio, pressure and feed tray location (Luyben, 2006).

3.1 Heterogeously catalysed and homogeneously catalysed RD

The application of catalyst to RD can either be heterogeneously or homogeneously catalysed RD. Although, heterogeneously catalysed RD portrays some advantages over homogeneously catalysed RD. The size and position of the reactive section in the column can be selected easily. More so, the separation and recycling of the catalyst can be circumvented (von Harbou, 2013).

Generally, two types of internals are utilised for heterogeneously catalysed RD processes. They are trays and catalytic packings. Krishna (2003) and Dörhöfer (2006) presented reviews on hardware selection for RD. Both types of internals are applicable for laboratory and industrial equipment. CATACOL (Axens, Rueil-Malmaison, France), KATAPAK-SP (Sulzer, Winterthur, Switzerland) (Götze et al., 2001) and D + R tray (BASF SE, Ludwigshafen, Germany) (Schmitt et al., 2009) are notable examples

comprised of traditional distillation trays and fixed bed reactors (von Harbou, 2013).

3.2 Types of reactive distillation systems

Various types of reactive distillation are utilised for a range of chemical reactions in reactive columns. Numerous types of process structures are also implemented; some have recycles of a reactant in excess while others do not have any reactant recycle. The most notable are: Single-feed reactions, irreversible reaction with heavy product and stable operation versus use of excess reactant (Luyben, 2006).

3.2.1 Single-feed reactions

In single-feed reaction, two products generated can be easily controlled and designed since the need to balance the stoichiometry is not compulsory.

$A \leftrightarrow B + C$

The two products are withdrawn from both ends of the column. Example of this type of RD is olefin metathesis. In Figure 3 below, A C_5 olefin undergoes reaction to produce a light C_4 olefin removed as the distillate, and a heavy C_6 olefin withdrawn as the bottom product. The feed flow controller (FC) regulates the production rate while the two temperature controllers are for adjusting conversion and product quality (Luyben, 2006).

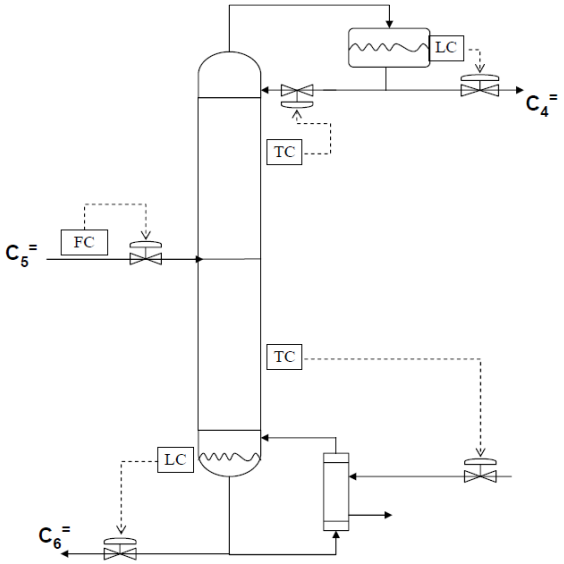

Figure 3: Olefin metathesis (Luyben, 2006)

3.2.2 Irreversible reaction with heavy product

This is a typical reactive distillation observed in the production of ethylene glycol, involving two reactants consumed in a rapid and irreversible reaction.

Ethylene oxide + water → ethylene glycol

This production process is illustrated in Figure 4. Ethylene oxide is a volatile gas, and ethylene glycol is a very heavy liquid. So the product is collected from the bottom of RD column (Luyben, 2006).

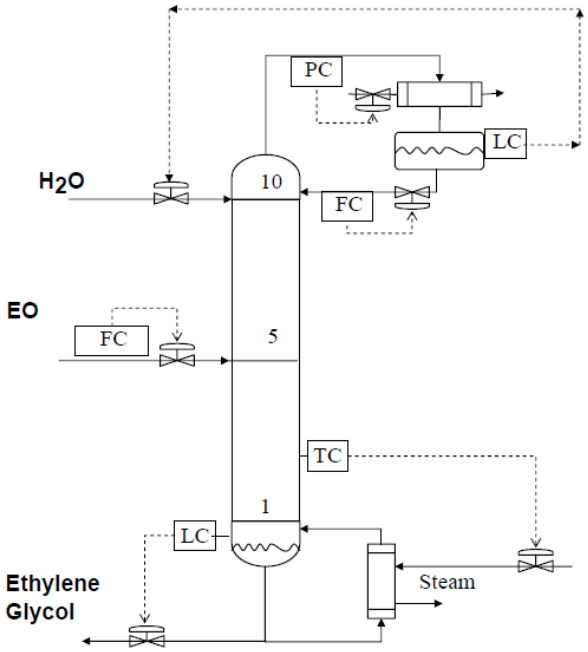

Figure 4: Ethylene glycol production with effective control system (Luyben, 2006).

3.2.3 Stable operation versus use of excess reactant

In reactions involving two reactant feedstreams, either of these two flowsheets is employed. For example, in the reaction below:

$$A + B \rightleftarrows C + D$$

One approach to design the process is by introducing one of the reactant in excess through the RD column. In Figure 5, an excess of reactant B was inserted into the column. Frequently, the excess reactant must be recovered. This operation is conducted in the recovery column which is the second distillation column. The recycle of B from the column is then mixed with new feed of B for the subsequent RD (Luyben, 2006).

The complete flow of B to the RD column is regulated by manipulating the new feed of reactant B. On the other hand, only one column can be employed in the flowsheet. This is more economical but much more problematic to control. This operation is “neat” because the quantities of the two reactants utilised are accurately balanced in order to fulfill the reaction

stoichiometry. Figure 6 portrays a system of a reaction that produces two products (A + B ⇄ C + D) collected at both ends of the column. The two temperature controllers (TC) provide information if additional or lesser amount of each reactant is required (Luyben, 2006).

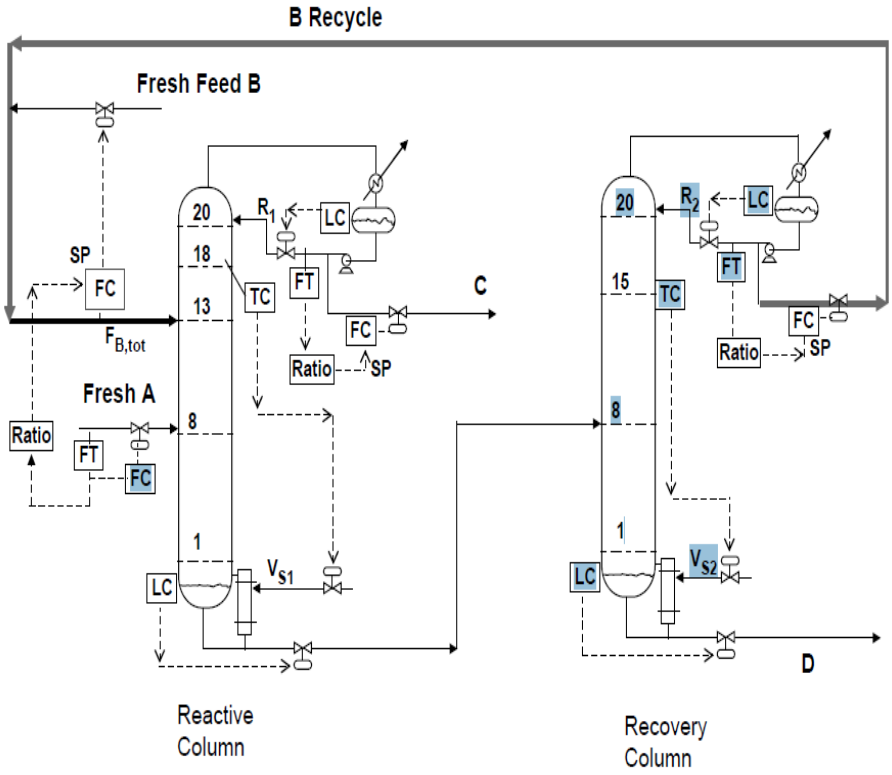

Figure 5: Excess of reactant B with the control units (Luyben, 2006).

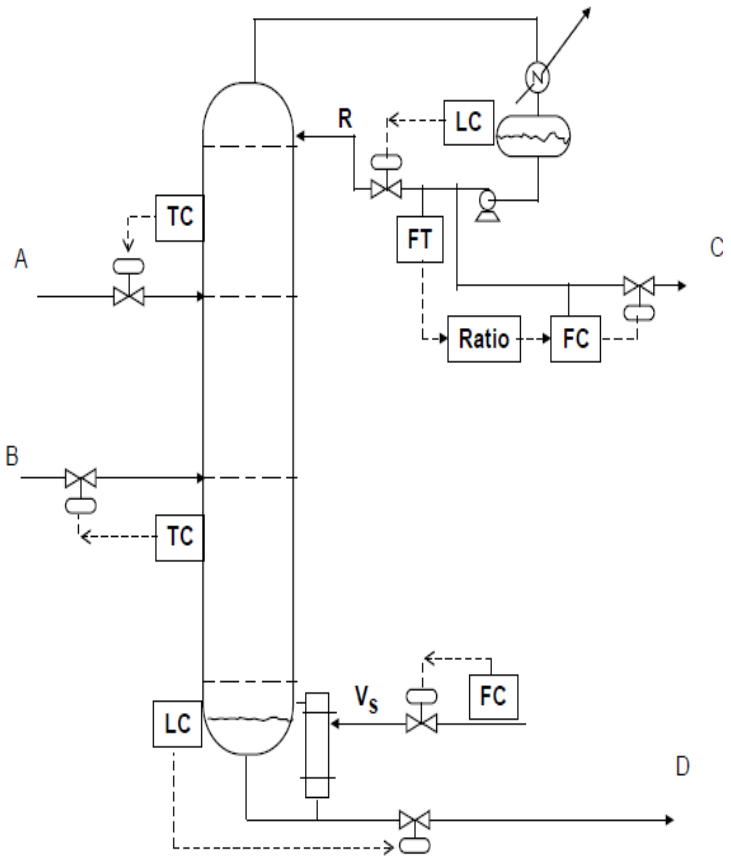

Figure 6: Neat operation with control units (Luyben, 2006).

4. Case study: etherification of 2-methoxy-2,4,4-trimethylpentane.

Tertiary ethers (fuel oxygenates) have had enormous impact on the upgrading of gasoline. They have been extensively utilised to increase the octane rating for the past 30 years. Ethers such as 2-methoxy-2-methylbutane (TAME), 2-ethoxy-2-methylpropane (ETBE) and the most extensively utilised, 2-methoxy-methylpropane (MTBE); were the most economically viable. Improvement of the octane rating leads to cleaner burning of gasoline, reducing harmful emissions from vehicles (Davis, 1999). Notwithstanding the rising percentage of ethanol direct blending, ETBE in gasoline pool is still promising (EFOA, 2010).

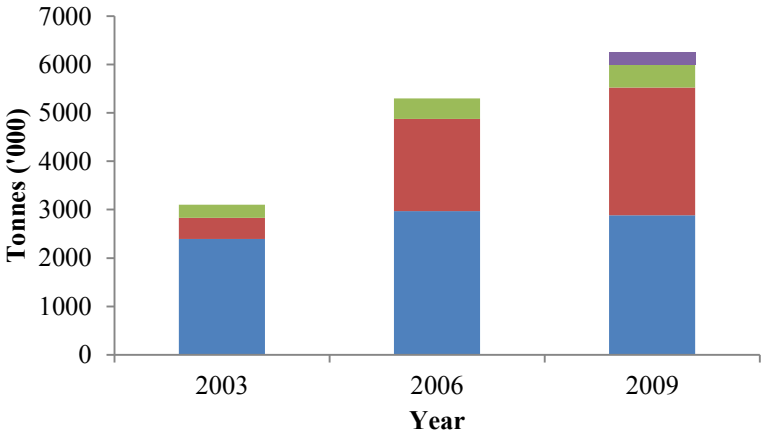

Figure 7: Fuel ethers demand in Europe (EFOA, 2010). ■, MTBE; ■, ETBE; ■, TAME; ■, TAEE;

4.1 Etherification of 2-methoxy-2,4,4-trimethylpentane

Sloan et al. (2000) suggested that existing MTBE plants could however be transformed to manufacture chemical such as 2,4,4-trimethyl-1-pentene (TMP-1) and 2,4,4-trimethyl-2-pentene (TMP-2), or the hydrogenated product of diisobutylenes, 2,4,4-trimethylpentane (a high quality fuel component isooctane).

Karinen et al. (1999) proposed that 2-methoxy-2,4,4-trimethylpentane (TOME) can be produced by etherification. The production process entails the dimerisation of isobutene in the presence of ion exchange resin catalyst to obtain iso-octenes (major components are TMP-1 and TMP-2). TMP-1 and TMP-2 react simultaneously with methanol to form TOME.

4.2 Physical properties of 2-methoxy-2,4,4-trimethylpentane

A precise knowledge of the vapour pressures and vaporisation enthalpies of alcohols, olefins and ethers are crucial for the optimal design of etherification processes. This will assist in the characterisation of various feeds utilised for dimerisation and etherification processes (Verevkin et al., 2003). The vapour pressures and vaporisation enthalpies of a range of olefins and alcohols have been investigated in Verevkin et al., 2000; Kulikov et al., 2001[a]; Kulikov et al., 2001[b]; Verevkin et al., 2003.

According to Uusi-Kyyny et al. (2001), the investigated density of TOME at ambient temperature (298.15 K) with an Anton-Paar-40 vibrating tube densimeter was 0.7930 g/cm^3. The same article also reported the vapour pressure of TOME.

Table 1: Vapour pressure data of TOME (Uusi-Kyyny et al., 2001).

T/K	**P/kPa**	**T/K**	**P/kPa**
417.95	100.56	376.76	29.78
416.10	95.75	371.61	24.95
413.91	90.52	365.16	19.8
411.51	85.16	360.89	17.00
409.20	80.09	355.67	13.93
407.00	75.11	351.12	11.66
404.43	69.90	345.16	9.16
401.70	64.86	339.93	7.33
399.15	60.08	336.52	6.29
396.18	55.03	335.13	5.94
392.97	49.98	333.35	5.47
389.59	45.10	331.13	4.94
385.68	39.89	329.11	4.49
381.61	34.98	326.45	3.96

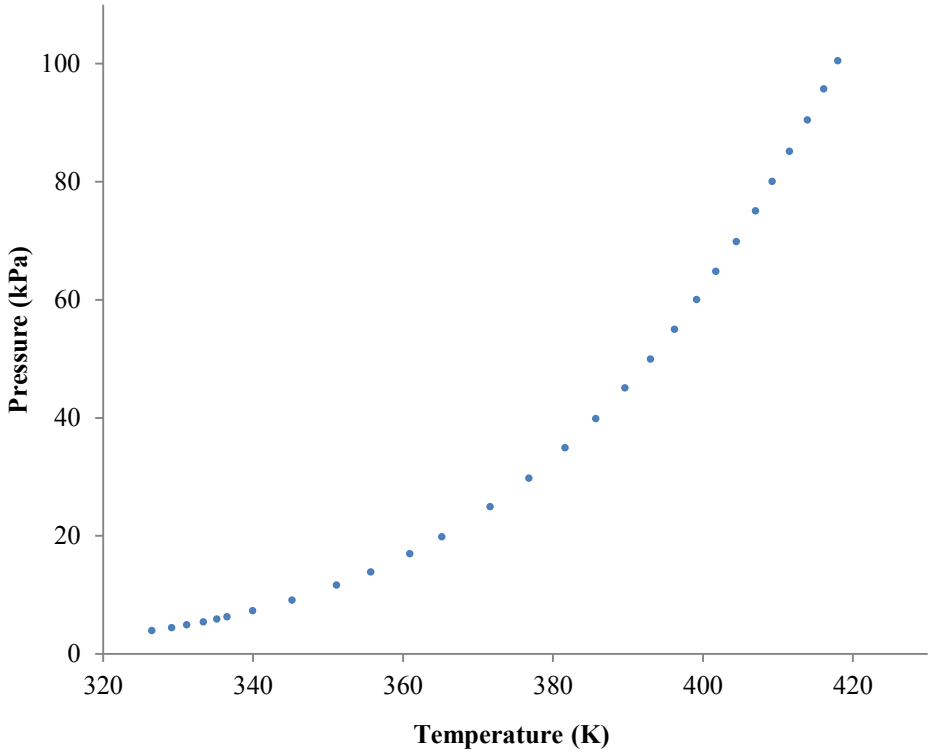

Figure 8: Measured vapour pressure of TOME (Uusi-Kyyny et al,. 2001).

, vapour pressure curve of TOME.

Also in earlier articles, TOME has been classified as a high octane rating chemical, possessing a blending motor octane number of 99, octane number of 147 and the blending research octane number of 110 (Karinen, 2002; Papachristos, 1991).

5. Phase equilibria

The modeling, measurement and calculation of multicomponent phase equilibria have imposed major challenges in chemical engineering. The numerous computational and experimental methods formulated by physical chemists and chemical engineers for thermodynamic description and measurement of vapour-liquid equilibria (VLE) possibly exceed that associated with other areas of chemical engineering research (Raal and Mühlbauer, 1998). The pursuit of fresh measurement techniques dates back to 1913. This was the period Jamaguchi (1913) and thereafter Sameshima (1918) designed the first recirculating stills utilised for low-pressure VLE measurement. Similarly, a number of methods have been created to portray the equilibrium conditions. A range of equations have also been formulated to describe the behaviours of the compositions which the system under investigation is composed of. Various problems in computational techniques and experimental methods hinder chemical engineers in this field (Raal and Mühlbauer, 1998).

A typical chemical plant is normally comprised of a preparation, reaction and separation stages. Though the reactor is regarded as the central unit of the chemical plant, however, over 60 % of total costs are accountable for by the separation steps. During separation, lots of energy is consumed to attain the desired purity level of products (Gmehling, 2006).

Separation processes like absorption, distillation, liquid-liquid extraction and stripping still prevail as the major unit operations regarding hydrocarbon separations. Regulations restricting the discharge of effluents (undesired components) into the environment, which must be at the minimal acceptable level, make these unit operations very significant. In addition, the condition required for ultrapure specialty substances also necessitate the utilisation of separation processes (Raal and Mühlbauer, 1998).

All the same, all these separation processes would be almost practically impossible to accomplish without a promising equilibrium distribution of components, in liquid-liquid or vapor-liquid streams as example.

Knowledge of phase equilibrium detail for a cost-effective separation process is paramount for process analysts and plant designers. In spite of the importance in proper knowledge of this phase equilibrium, reports suggest that most engineers entrusted with process design and development lack adequate skills in either the proper approach to execute physical property measurements or thermodynamics, or both. According to Kistenmacher (1995), numerous phase equilibrium data collections are unreliable. Alternatively, this might be largely due to errors in measured compositions, temperature and pressure of available data. This will however impose further obstacles on plant engineers. In order to circumvent these problems, phase equilibrium data measurements are usually accredited to specialist firms or institutions (Raal and Mühlbauer, 1998).

5.1 Phase equilibrium conditions

The conditions for equilibrium are that both temperature and pressure for each phase (α and β) must be identical. In addition, the chemical potential or fugacity of each component, *i*, in each of the phases must be equal. (Raal and Mühlbauer, 1998).

$$T^{\alpha} = T^{\beta} \tag{4.1}$$

$$p^{\alpha} = p^{\beta} \tag{4.2}$$

$$\mu_i^{\alpha} = \mu_i^{\beta} \tag{4.3}$$

The chemical potential is also equivalent to the partial molar Gibbs energy (Gmehling, 2012).

$$\mu_i = \bar{g}_i \tag{4.4}$$

More so, the partial molar Gibbs energy could also be represented by the fugacity thus;

$$\bar{g}_i(T, P, z_i) = \bar{g}_i^{pure}(T, P^{\circ}) + RTIn\frac{f_i(T,P,zi)}{f_i{}^{\circ}(T,P^{\circ})} \tag{4.5}$$

The properties $g_i^{pure}(T,P^\circ)$ and f_i° of pure component are functions of pressure and temperature only; they therefore have the constant values in all phases (Gmehling, 2012).

Similarly, the conditions to achieve phase equilibrium can also be denoted by fugacity as follows;

$$\bar{g}_i^\alpha = \bar{g}_i^\beta \tag{4.6}$$

$$f_i^\alpha = f_i^\beta \tag{4.7}$$

Equation (4.7) above is the starting point for thermodynamics of mixtures and practically all phase equilibrium computations.

As pressure tends to zero, fugacity becomes equivalent to the partial pressure.

$$\lim_{p\to 0} \frac{f_i}{z_i p} = 1 \tag{4.8}$$

The reference state in equation (4.5) is pure substance. Comparably, it can be demonstrated as;

$$\bar{g}_i(T,P,z_i) = \bar{g}_i^\circ\left(T,P^\circ,z_i^\circ\right) + RTIn\frac{f_i(T,P,z_i)}{f_i(T,P^\circ,z_i^\circ)} \tag{4.9}$$

When two phases are being considered, the equilibrium condition is achieved thus;

$$\bar{g}_i^{\circ\alpha}\left(T,P^\circ,z_i^{\circ\alpha}\right)RTIn\frac{f_i^\alpha(T,P,z_i^\alpha)}{f_i^{0\alpha}(T,P^{0\alpha},z_i^{0\alpha})} = \bar{g}_i^{\circ\beta}\left(T,P^{\circ\beta},z_i^{\circ\beta}\right) + RTIn\frac{f_i^\beta(T,P,z_i^\beta)}{f_i^{0\beta}(T,P^{0\beta},z_i^{0\beta})} \tag{4.10}$$

When the reference states $(P^{\circ\alpha},z_i^{\circ\alpha})$ and $(P^{\circ\beta},z_i^{\circ\beta})$ are unidentical, equation (4.10) becomes:

$$\bar{g}_i^{\circ\alpha}\left(T,P^\circ,z_i^{\circ\alpha}\right) = \bar{g}_i^\beta\left(T,P^{\circ\beta},z_i^{\circ\beta}\right) + RTIn\frac{f_i^\beta(T,P,z_i^\beta)}{f_i^{0\beta}(T,P^{0\beta},z_i^{0\beta})} \tag{4.11}$$

This also results into (Gmehling, 2012):

$$f_i^{\alpha}(T,P,z_i^{\alpha}) = f_i^{\beta}(T,P,z_i^{\beta}) \tag{4.12}$$

In the subsequent paragraphs, phase equilibrium (liquid-liquid equilibrium and vapor-liquid equilibrium) concepts will be discussed in more detail.

5.2 Liquid-liquid equilibrium (LLE)

The occurrence of two-phase liquid (or more) inside a binary or multicomponent system has distinguished practical interpretation for industrial unit operations. In distillation for example, systems or conditions which might result in liquid-phase immiscibility are frequently avoided because they influence plate efficiency, capacity and control of phase are very demanding. Pumping is also generally avoided for two-phase liquid systems. On the contrary, liquid-liquid extraction, an effective and generally energy-efficient separation process employed for dilute aqueous solutions is dependent on dispersion of solute between immiscible liquid phases. LLE are controlled by temperature while pressure effect is minimal (Raal and Mühlbauer, 1998).

Recalling the condition necessary for phase equilibrium, equation 4.13 below could be modified to obtain the activity coefficient (γ) relationship (Gmehling, 2012 and Robles, 2009).

Standard state fugacity for the two liquid phases is constant.

$$f_i^{I}(T,P,x^{I}) = f_i^{II}(T,P,x^{II}) \tag{4.13}$$

$$(x_i\gamma_i f_i^{0})^{I} = (x_i\gamma_i f_i^{0})^{II} \tag{4.14}$$

$$x_i^{I}\gamma_i^{I}(T,P,x^{I}) = x_i^{II}\gamma_i^{II}(T,P,x^{II}) \quad i=1,2,3\ldots \tag{4.15}$$

The activity coefficient can be ascertained utilising suitable thermodynamic model (Robles, 2009). Equation 4.15 above can also be expressed in terms of activity ($a_i = x_i\gamma_i$) meaning that isoactivity exists in the two phases.

5.3 Vapour-liquid equilibrium (VLE)

According to Sandler and Orbey (1998), equation 4.12 which is the initial step for VLE computation is modified below for VLE measurement;

$$\overline{f}_i^L(x_i, T, P) = \overline{f}_i^V(y_i, T, P) \tag{4.16}$$

Subscripts x and y represent the mole fraction of species i. Superscript L and V are liquid and vapour phases. Equation of state (EOS) model is usually employed for the derivation of the fugacity in the vapour phase as a function of composition, temperature and pressure. However, the liquid phase fugacity can be determined by two methods; using the EOS for both phases or utilising the activity coefficient model. The last approach is termed the Gamma-Phi method, γ-ϕ method. This means that activity coefficient model is used for the liquid phase while EOS model is employed for the vapour phase fugacity coefficient. When EOS is applied to compute the fugacity of both phases, this is referred to as the ϕ-ϕ method.

5.4 Gamma-Phi method for VLE

The fugacity in a vapour can be calculated from the expression between the Gibbs free energy, fugacity and an equation of state as follows (Sandler and Orbey, 1998);

$$In\left[\frac{\overline{f}_i^V(T,P,y_i)}{y_i P}\right] = In\overline{\Phi}_i$$

$$= \frac{1}{RT}\int_{V=\infty}^{V}\left[\frac{RT}{V} - \left(\frac{\partial P}{\partial N_i}\right)_{T,V,N_{j\neq 1}}\right]dV - In\,Z^V \tag{4.17}$$

V in this equation is the total volume and Z is compressibility factor. $Z = P\bar{V}$/RT is normally computed from EOS. Here $\bar{V}$ is the molar volume. One of such EOS is the virial equation.

$$\frac{P\overline{V}}{RT} = 1 + {}^{B(T)}\Big/_{\overline{V}} + {}^{C(T)}\Big/_{\overline{V}^2} + {}^{D(T)}\Big/_{\overline{V}^3} \qquad (4.18)$$

Coefficients B, C and D are the second, third and fourth virial coefficients. In a pure fluid, they are only a function of temperature. On the other side, in a mixture, they are functions of both temperature and number of mole. Another commonly used EOS based on van der Waals equation is Peng-Robinson (1976) equation.

$$P = \frac{RT}{\bar{V} - b} - \frac{a(T)}{\bar{V}(\bar{V} + b) + b(\bar{V} - b)} \qquad (4.19)$$

In this two-parameter cubic equations, *a* is temperature-dependent. Also, a and b are both dependent on the composition in a mixture. The root corresponding to largest molar volume is used to compute the vapour-phase fugacity.

For the calculation of VLE at low pressures using γ-ϕ method, equation below has to be resolved;

$$\bar{f}_i^L(T, P, x_i) = \bar{f}_I^V(T, P, y_i) \approx y_i P \qquad (4.20)$$

To describe fugacities in the liquid phase based on composition, an activity coefficient or an excess Gibbs free-energy model is usually employed. The relationship that connects the molar excess Gibbs free-energy of mixing ($\bar{G}^{ex}$), the activity coefficient(γ_i) and partial molar excess Gibbs free energy of a species ($\bar{G}_i^{ex}$) is shown below;

$$\overline{G}(T, P, x_i) = \bar{G}^{ex}(T, P, x_i) + \bar{G}^{IM}(T, P, x_i \qquad (4.21)$$

$$= \bar{G}^{IM}(T, P, x_i + \sum_i x_i \bar{G}_i^{ex}(T, P, x_i)$$

$$= \bar{G}^{IM}(T, P, x_i) + RT \sum_i x_i In\gamma(T, P, x_i)$$

The fugacity of a species in a liquid mixture is computed thus;

$$\bar{f}_i^L(T,P,x_i) = x_i\gamma_i(T,P,x_i)f_i^L(T,P) \quad (4.22)$$

In equation 4.22, $f_i^L(T,P)$ represents the fugacity of pure component *i* like a liquid at the pressure and temperature of the mixture.

The fugacity of a pure liquid at its saturation point is equivalent to its vapour pressure as long as the saturation pressure is low.

$$f_i(T,P) \approx P^{vap}(T) \quad (4.23)$$

At elevated vapour pressures, the fugacity coefficient is introduced and should the liquid be at pressure exceeding its vapour pressure, Poynting correction is also added (Sandler and Orbey, 1998).

$$f_i(T,P) = P^{vap}(T)\emptyset_i\left(T,P^{vap}(T)\right)\exp\left[\int_{P^{vap}}^{P}\frac{\bar{V}_i^L}{RT}dP\right] \quad (4.24)$$

$$\text{POY} = \exp\left[\int_{P^{vap}}^{P}\frac{\bar{V}_i^L}{RT}dP\right]$$

The Poynting correction in equation 4.24 is the exponential term. Poynting correction increases with increasing pressures (or decreasing temperature) (Raal and Mühlbauer, 1998).

6. Separation processes

Laboratory experiments are continuosly demanded and indispensable for research institutes and chemical industries. However, conventional batch-wise flasks and test tubes are being replaced with micro-reactors that offer online-analysing possibility and high throughput screening for novel processes and products (Angelescu, 2010; Arora, 2010; Barrow, 2011; Matawari, 2011; and Ziogas, 2012). In addition, micro-reactors are applied for the manufacture of test batches. They are utilised for full production in centimeter cubed per seconds (cm^3/s) flow rate (Calabrese, 2011; Hartman, 2009; Hessel, 2007; Kockmann, 2011; Kuhn, 2011; and Roberge, 2008).

In Gaakeer et al. (2012), the advancement of micro-reactors in chemical engineering processes also brings the requirement for micro-structured separation into limelight. This facilitates the development of new methods of separation. This is due to the influence surface forces imposes on these small devices in contrary to conventional operations which are mainly governed by density differences and gravitational forces.

6.1 Micro-distillation

The major phenomenon in distillation is continuous contact of vapour and liquid (Sundberg, 2012). Distillation is basically employed for separation of a component from a mixture based on boiling point differences. Batch distillation is a kind of distillation which involves heating of a liquid mixture to produce vapour, condensation of the vapour to liquid and withdrawal of the condensed liquid. On the contrary, continuous distillation entails partial vaporisation of a liquid mixture. The vapour is then separated by a flash drum from the liquid stream (Sundberg, 2012).

During process development of a new concept, good engineering practice often involves operation at smaller scale prior to the commercial scale plant. The separation method employed for both pilot plant and commercial scales should be alike in all ramifications to avert erroneous scale-up decisions.

This is however an uphill requirement to accomplish as there are limited studies in the field of micro-distillation. This might hinder minimisation of pilot plants. Very often in chemical processes, impurities exist in the feed which are unrecognisable during initial process development which might be due to their amounts being below the detection limit. Detection of these pitfalls among other difficulties for the complete piloting phase of process development is of utmost importance (Sundberg, 2012).

Attempts towards the development of micro-distillation are generally few despite its potential uses. One of such is the collimator-type distillation column (Fink and Hampe, 2000). The surface area-to-volume ratio of this column was large, inhibiting the regulation of the unit as a result of external heat losses. An increment of the heating duty merely resulted to drying out of the hot terminal. On the contrary to distillation column size and liquid film thickness, the sensor size was as well massive, thereby compounding the operating difficulties.

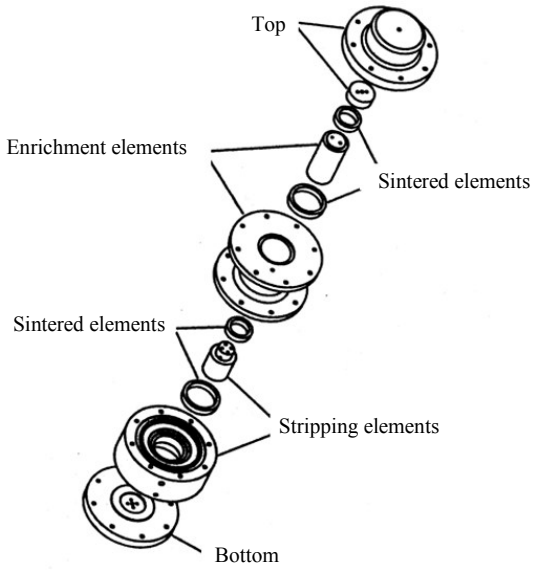

Figure 9: Scheme of a collimator-type distillation column (Fink and Hampe, 2000).

Seok and Hwang (1985) developed heat-pipe type distillation column possessing a glass tube with inside diameter of 10.5 mm and length of 540 mm. The column orientation was almost horizontal and was modeled by (Ramirez-Gonzalez, 1992 and Tscheenjaew, 1996).

There was reported attempt by Velocys Inc. (Tonkovich, 2007) to commercialize micro-scale distillation with acetone-water system having HETP of about 6 mm. The flow of liquid and vapour were in vertical direction. The difficulties of heat losses were however resolved by integrating various distillation columns inside particular unit.

The aforementioned distillation methods discussed are categorised according to separation efficiency of a single unit. The two modes of operation (concurrent and countercurrent) in micro-distillation will be elucidated in the subsequent paragraphs.

6.1.1 Concurrent (one-stage) micro-distillation

Boyd (2008) exhibited separation on nanoscale. The experiment was conducted using a 5-μm high and 30-μm wide micro-channel shielded with PDMS and enclosed with a glass substrate. The glass substrate was encrusted with gold nanoparticles. The channel was heated utilising a laser emanating light at 532-nm wavelength which excited the nanoparticles in a circular area of diameter 10 μm. Vaporisation and condensation of heated liquid emerged 10-20 μm farther, thereby entangling a gas bubble within the liquid. The gas bubble mitigated diffusion but enhanced vaporisation and condensation across. Figure 10 below depicts the process. The device was investigated employing a mixture comprised of ethanol, deionised water and dye mixture. The dye consisted of Coumarin 4 buffered with tris(hydroxymethyl)aminomethane and HCl. During the study, only ethanol and water navigated the barrier, neglecting dye mixture behind, though concentrations were not ascertained. The vaporisation rate was 0.75 pg/s. The procedure can be employed for the pre-concentration of temperature-sensitive components like biomolecules.

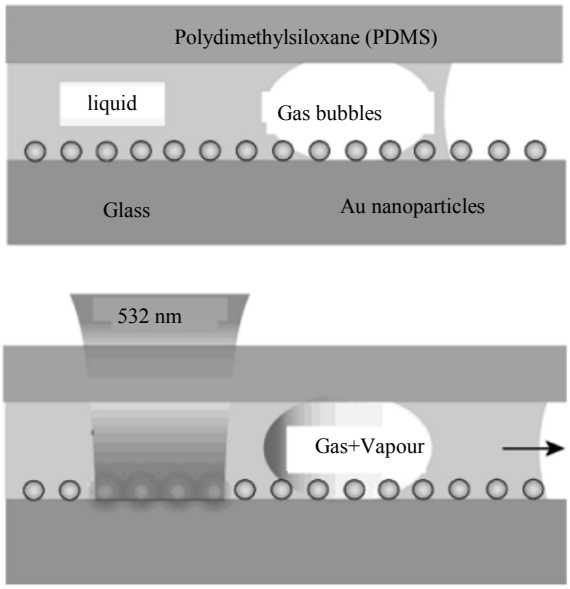

Figure 10: Diagrammatic representation of the micro-channel and the technique of separation involving bubble-assisted interphase mass transfer (Boyd, 2008).

In Hartman et al. (2009), micro-channel distillation was developed on the principle of segmented flow with carrier gas. The micro-channel fabricated with etching on a silicon substrate and rectangular in shape possessed a cross sectional area of 0.4×0.4 mm^2 and length of 0.87 m. The feed mixture was introduced into a nitrogen stream operating as a carrier gas at the beginning of the channel. The two phases produced apportioned flow with slugs transiting between gas bubbles. There was preheating of the flow inside the channel with the aid of electric heater partially flashing the liquid which is later separated by a membrane. Experiments performed employed binary mixtures of toluene-dichloromethane and methanol-toluene as feed.

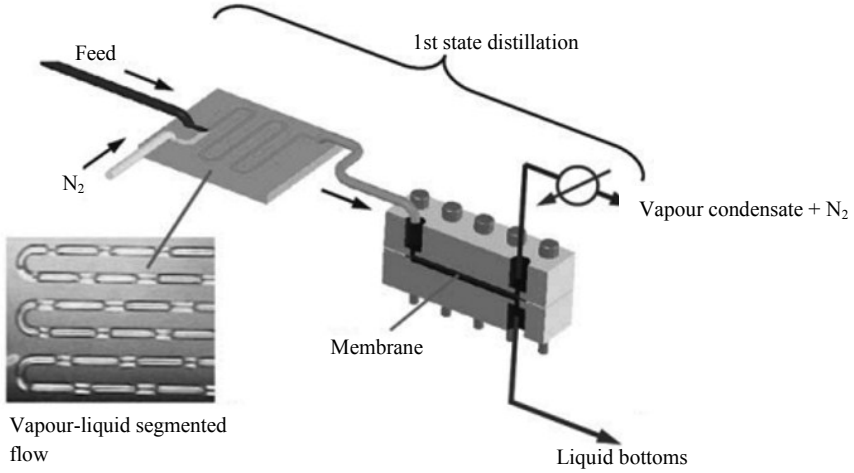

Figure 11: Schematic diagram of the vapour-liquid segmented-flow separation procedure (Hartmann, 2009).

Sotowa and Kusakabe (2003) assembled a micro-constructed single-stage contacting instrument. Vapour-liquid separation was realised in a flash chamber. The separation was gravity-dependent. Formation of vapour phase was executed by heating the device inside a water bath. A number of channel cross-sections from 137×137 μm^2 were developed and investigated. Experiments administered were by 70 mol-% aqueous methanol solution at water bath temperature of 72 °C. Feed flow rates were 0.02 cm^3/min and 0.1 cm^3/min with corresponding separation efficiencies of 0.80 and 0.65 ideal stages.

Nanoscale vapour-liquid equilibrium seems practically impossible to accomplish as demonstrated by Boyd et al. and other reported paper (Hibara, 2008). The undetermined problems associated with removal of one of the products; therefore they resemble batch distillation more than continuous-flow separation.

6.1.2 Countercurrent micro-distillation

Tonkovich (2009) demonstrated a distillation column composed of multiple separation segments. Liquid and vapour flows were in countercurrent direction. A modification of the column comprised of a laminated structure

having heat exchange channels within the distillation channels. Figure 12 below portrays a microscale distillation single channel. Fanelli (2009) modeled the operation of this unit using mixture of cyclohexane and hexane was conducted. There was downward movement of liquid when falling film became steady in a 178 μm thick steel mesh. Vapour movement was upward inside an open channel with thickness of 1.33 mm. Feed flow rate of 1 cm^3/min of a hexane-cyclohexane system generated height equivalent to theoretical plate (HETP) of 21 mm.

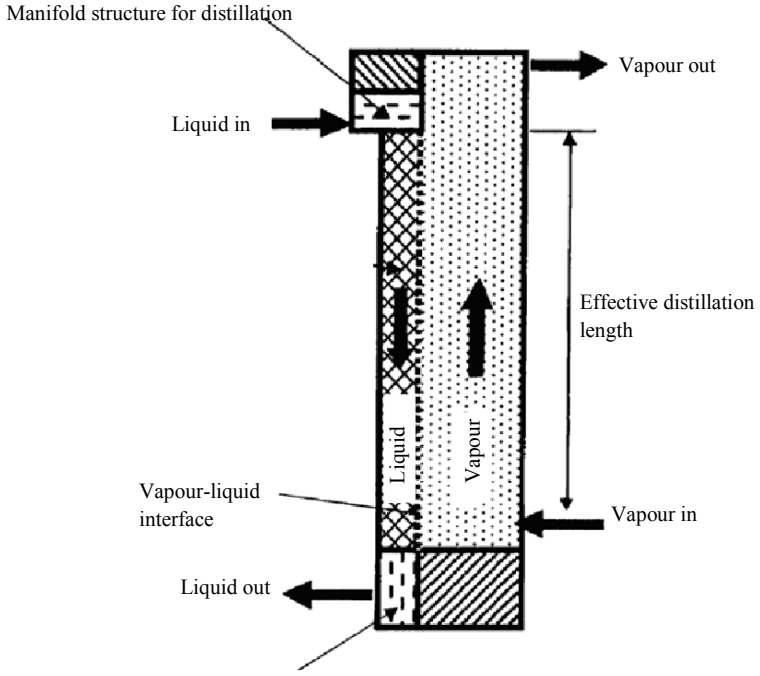

Figure 12: Schematic of micro-scale distillation channel described by (Tonkovich, 2009)

MacInnes (2010) reported a novel device utilising a spinning spiral micro-channel to produce multistage separation**.** The micro-channel was cut in resemblance of a spiral on a glass disc and subsequently bonded onto another one. The channel was 250 μm wide, 95 μm in depth with length of the contacting channel as 35.3 mm. Introduction of feed from a reservoir to the middle of the disc was by tubing possessing internal diameter of 150 μm. The speed of rotation of the disc during operation was 5000 rpm. The

products were collected into a 50 μm diameter from the edge of the disc into two vessels. The diagram of this device is illustrated in Figure 13.

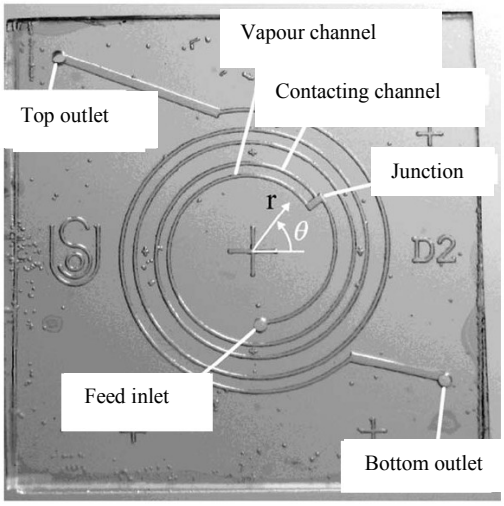

Figure 13: Schematics of spinning spiral micro-distillation column (MacInnes, 2010).

7. Gas chromatography

Gas chromatography (GC) and liquid chromatography are presently the most popularly utilised equipment for analysing chemical compositions of multicomponent organic mixtures. GC units employed alone for analysis in the United States exceed 250,000. Capillary and packed columns and operating conditions have been greatly developed for separating the compositions of mixtures. After separation, quantitative analysis can be accomplished utilising a number of extremely efficient and specialised detectors. Columns can be utilised in series for intricate separations, and many detectors can also be employed simultaneously. The flame ionisation detector, very sensitive to molecules possessing specifically C-H bond, have the ability to detect flows as low as 10^{-11} g/s. In GC analysis, information about composition is not provided, whereas, only peaks areas are generated, corresponding to quantities of the various substances (Raal and Mühlbauer, 1998).

For liquid mixtures, substantial accuracy and reliability in calibration is achievable by preparing and analysing standard solutions weight measurement. Description of the distinct procedure for GC detector calibration is presented. Depending on the type of detector, frequent recalibration might be necessitated, prompting an efficient and accurate procedure (Raal and Mühlbauer, 1998).

7.1 Response factor

The definition of response factor (F) was stated in Raal and Mühlbauer (1998). This is the proportionality constant between the number of moles transiting the detector and the peak area, A attained from an electronic integrator (Perry 1981): $n_i = A_i F_i$. As long as the area, A relies on the quantity of sample introduced, but not generally highly reproducible, so it is judicious to work only with area ratio, as follows;

$$\frac{n_1}{n_2} = \frac{A_1}{A_2} \cdot \frac{F_1}{F_2} = \frac{x_1}{x_2} \qquad (7.1)$$

x=mole fraction

The response factor ratio (F_1/F_2) is generally not constant throughout wide composition ranges, also in a situation whereby very small liquid sample (about 0.30 µl) is inserted, for detector overloading prevention. Hence, it is pertinent in mixture calibration "to plot area ratios for pairs of components versus their mole fraction ratios". An example is displayed below for cyclohexane-ethanol binary system in Figures 14 and 15. Component 1 is selected as the one present in larger amount in moles. Steady response factor ratios occur when the slope of Figure 14 equals the inverse of the slope of Figure 15. For a multicomponent system, if the preceding statement is fulfilled for a binary pair, the response factor ratios are directly and simply related (Raal and Mühlbauer, 1998).

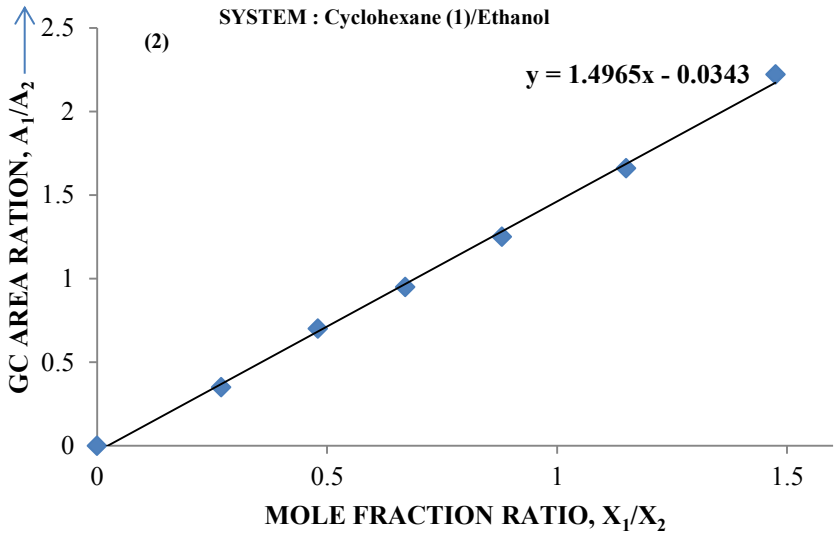

Figure 14: Example of GC detector calibration for an ethanol(2)/cyclohexane(1) binary mixture in low cyclohexane concentration region (Raal and Mühlbauer, 1998).

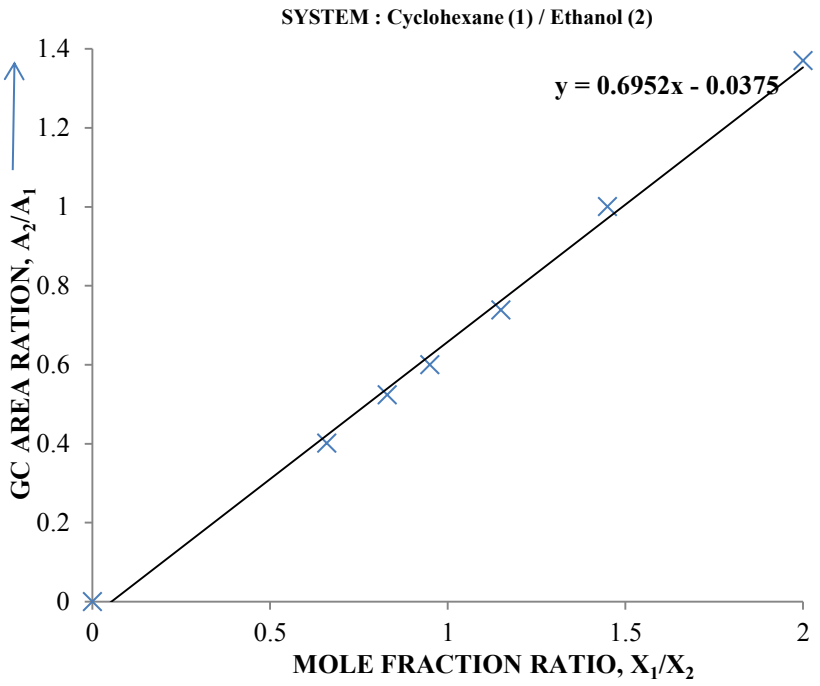

Figure 15: GC detector calibration for an ethanol(2)/cyclohexane(1) mixture in low ethanol concentration region (Raal and Mühlbauer 1998).

7.2 Determination of compositions of a sample

For a binary system, component 1 (desired component) and component 2, which might be the second component or the impurity of the system, the actual mole fraction of component 2 can be ascertained firstly by deriving the GC areas A_1 and A_2 (Raal and Mühlbauer, 1998). According to Grob and Barry (2004), the response factor of component 2 can be calculated thus;

$$F_2 = \frac{m_2}{m_1}.\frac{A_1}{A_2} \qquad (7.2)$$

Hence, liquid or vapour composition of component 1 can be computed as follows;

$$x_1 = \frac{A_1/M_1}{A_1/M_1 + F_2 A_2/M_1} \quad (7.3)$$

Where m_1 and m_2 are masses of gravimetrically prepared components in a sample and M_1 and M_2 are their corresponding molar masses.

8. Chemicals

Pure methanol produced by SIGMA ALDRICH was utilised for this experiment and analysed by gas chromatography (GC). The water content of the methanol determined by Karl Fischer (KF) was 0.023 %. Diisobutylene (3 parts TMP-1 and 1 part TMP-2) with 97 % purity also investigated by GC was manufactured by SIGMA ALDRICH.

Table 2: The area percent GC report for the examined methanol sample.

Signal 1: FIDI A					
Peak	**RetTime**	**Width**	**Area**	**Height**	**Area**
#	[min]	[min]	[pA*s]	[pA]	%
1	5.00	0.05	62600	19500	100

Table 3: The area percent GC report for the analysed diisobutylene sample.

Signal 1: FID1 A,					
Peak	**RetTime**	**Width**	**Area**	**Height**	**Area**
#	[min]	[min]	[pA*s]	[pA]	%
1	1.34	0.06	358	96	0.143
2	8.45	0.13	1729	182	0.687
3	9.44	0.09	194000	3	77.004
4	9.59	0.04	804	349	0.319
5	9.78	0.06	5	13300	20.258
6	9.98	0.04	664	262	0.264
7	10.05	0.04	2733	1023	1.086

From Table 2, the retention time of methanol is 5.00 min. The area percent shows that only methanol is present as reported by the manufacturer. Similarly, from the GC result of Table 3, the retention times of TMP-1 and TMP-2 are 9.44 min and 9.78 min sequentially. The sum of the area percent (77.0 % and 20.2 %) of these two compounds corroborates the 97 % purity. Peak 1 that appeared on the GC report is an impurity while the other four

peaks (2, 4, 6 and 7) on the GC analysis are diisobutylene isomers, also regarded as impurity for this process. The retention times of methanol, TMP-1, TMP-2 and the other diisobutylene isomers from Tables 2 and 3 are useful in the identification of these components in subsequent GC result of RD samplings.

9. Apparatus

The parts constituting the micro-plant have been elucidated in section 2.2 of this research. However, the reactive distillation column employed has two ideal stages, operating with negligible pressure drop. The round bottom flask containing the feed volume is 1 dm^3. A small magnetic stirrer is inserted to improve mixing in the system. The experimental diagram is presented below in Figure 21. For temperature measurements at three different points, temperature meter manufactured by Nokeval with platinum (PT-100) was utilised. The Nokeval data logger, magnetic stirrer and heating system were activated. The measured temperatures displayed on the data logger are inspected during the experiment.

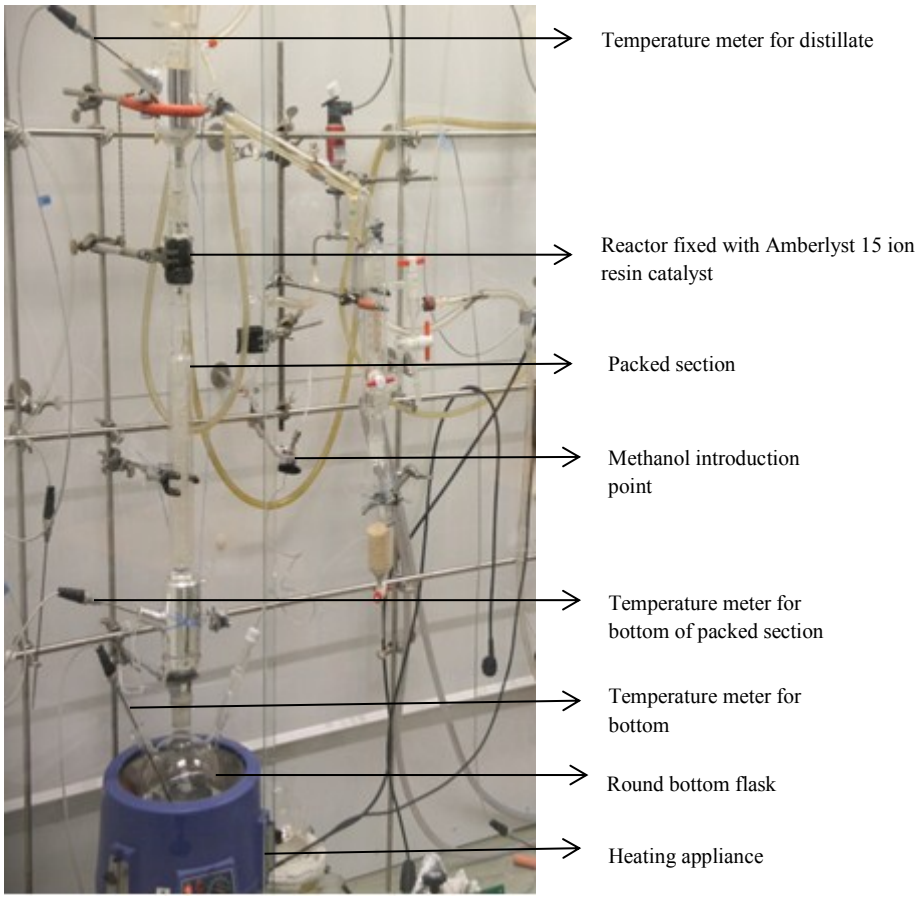

Figure 21: The reactive distillation column used by chemical engineering research group, Aalto University. The initial feed is usually introduced through any of the three openings of the round bottom flask. Mass transfer was executed in the column by 6 mm × 6 mm Raschig-ring packing.

10. Phase equilibrium and simulation

The boiling points of the main components involved in TOME production (TMP, methanol, DME and TOME) are far from one another: MeOH = 337.5 K (Luyben, 2010), TMP-1 = 374.59 K (Danner and Daubert, 1992), DME = 248.2 K (Luyben, 2010) and TOME = 417.95 K (Uusi-Kyyny et al., 2001). Fortunately, DME which is the side reaction product manufactured along with TOME is found at the top of the distillation column during RD owing to its low boiling point and VLE behaviour. At elevated temperature, unreacted methanol also migrates to the top of the column. This makes the separation of the other components in the bottom moderately comfortable.

Prior to the commencement of RD runs, VLE data for methanol and 2,4,4-trimethyl-1-pentene system available in (Uusi-Kyyny et al., 2001) was reviewed to determine the operating condition required for the system. Between temperatures of 332 K and 337 K, methanol and diisobutylene binary system form azeotropic compositions. The mole fraction of methanol in the liquid phase, $x_{azeotrope}$(methanol), at these two temperatures are 0.771 and 1 respectively. It was then agreed to keep the operating temperature above 343.15 K (70 °C) at atmospheric pressure.

In addition, it is also crucial to regulate dimethyl ether (DME) formation from the side reaction of the decomposition of methanol in this process. This was implemented by applying only a fraction of methanol required in the reactant feed to diisobutylene. In reality, the stoichiometric ratio of the two reactants is 1:1. This is clarified in subsequent procedure section. Also, equation showing methanol decomposition is below.

DME formation

$$2\ CH_3OH \rightarrow H_2O + CH_3OCH_3 \qquad [10.1]$$

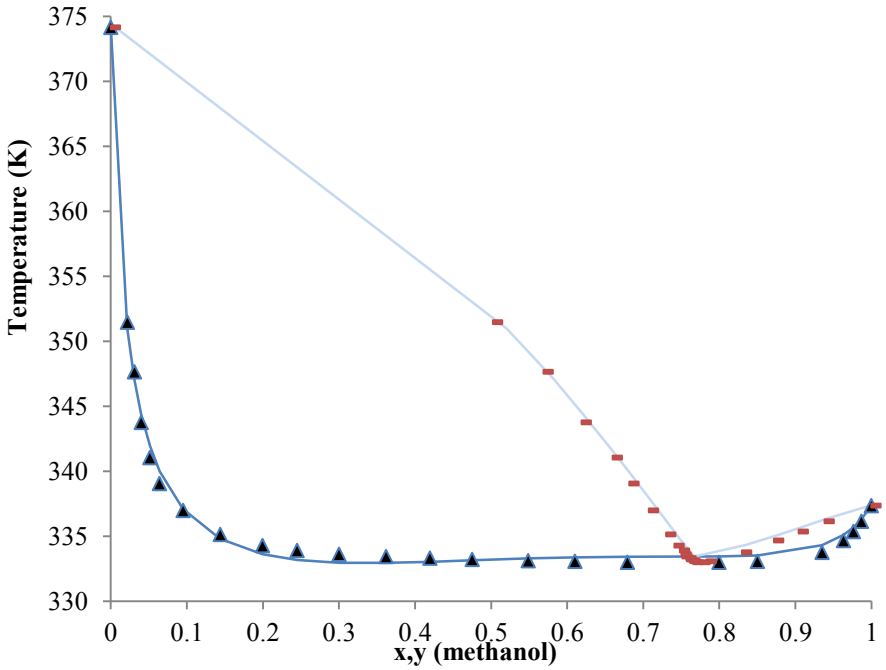

Figure 21: The phase diagram (T-xy diagram) of methanol and 2,4,4-trimethyl-1-pentene system (Uusi-Kyyny et al., 2001), regressed with NRTL model of Aspen Plus. , Tx-measured; , Ty-measured; , Tx-model; , Ty-model.

11. Experimental Procedure and analysis

11.1 Experimental procedure

During the micro-plant runs, 0.50 dm^3 feed of diisobutylene and methanol at different percentage compositions was usually utilised. The pump controller, syringe pump, reactor pre-heater temperature control unit and reactor temperature controller were activated. The reactor pre-heater and reactor temperature controllers were adjusted to the desired operating temperature of the process. The feed in a reagent bottle was introduced via the pump controller at flowrate of 10 cm^3/min until 80 cm^3 of the feed is present in the pump. About 10 cm^3 in the pump was returned back into the feed container because there are usually some air bubbles present. The pump is refilled over and over again until it was devoid of air bubbles. The valve that leads into the reactor is opened and the feed was introduced into the reactor. After the reactor was completely filled, the pump controller was modified to inject the remaining feed in the glass container at flowrate of 0.10 cm^3/min into the reactor through the pump. As the reaction progressed, the product from the reactor was analysed by gas chromatography connected to the micro-plant. Nitrogen is introduced into the system to obtain one phase (liquid phase) system.

For the first RD run, the feed composition (0.50 dm^3) of 9.90 mol-% of methanol and 90.10 mol-% of diisobutylene when analysed by GC resulted into 8.80 mol-% methanol and 91.21 mol-% diisobutylene. The feed was then introduced into a 1 dm^3 round bottom flask. After the introduction, the reboiler was switched on to heat the feed. The heating power was adjusted to the desired point. The process was conducted at isobaric pressure (atmospheric pressure). Online temperature measurement at three different points during the experimental run was recorded. The steady state was accomplished in about an hour. When methanol in the feed was consumed, noticeable by continuous temperature rise in the temperature of the column, 9.90 g of methanol was injected into the bottom. Subsequent additions of methanol administered into the column were 8.80 g, 7.80 g and 6.90 g.

Table 4: The area percent GC report of the feed for RD run 1.

Peak	RetTime	Width	Area	Height	Area
#	[min]	[min]	pA*s	[pA]	%
1	5.02	0.03	1642	782	0.957
2	9.25	0.09	763	130	0.445
3	9.48	0.08	131000	24100	76.422
4	9.64	0.03	551	239	0.322
5	9.83	0.05	34800	10165	20.287
6	10.03	0.04	449	178	0.262
7	10.10	0.04	1860	703	1.083
8	10.32	0.04	383	161	0.223

11.2 Analysis

The same GC was utilised for analysis of micro-plant and RD samples. Samples were investigated by Agilent 6850 series gas chromatograph system, Agilent 7683 series injector and an autosampler in the VLE laboratory. A capillary column (HP-1, cross-linked methylsiloxane); 60 m length, 0.25 mm internal diameter and 1.00 μm film thickness. The detector employed was flame ionisation detector. Helium was utilised as the carrier gas. The response factors of MEOH, TMP-1, TMP-2 and TOME were used to correct GC results. This is because the use of one detector and another to determine the spectral peak of a compound will produce different results. Response factors are calculated for each compound present in a sample for a particular detector. From the computed response factors, the actual compositions of the analysed sample could be ascertained with equation 7.2 in chapter 7 of this research.

12. Experimental runs and results

The experimental result presented in this thesis is divided into two parts. Firstly, production of TOME was demonstrated with the application of reactor of the micro-plant without putting the micro-distillation unit into use for purification. On the other hand, the second section involves the utilisation of reactive distillation mechanism for the production of TOME.

The experimental results of micro-plant reactor runs without the application of micro-distillation for purification are presented in this section. Usually the experiments were conducted for about 20 hours or more. Even at night, the experimental runs were still ongoing without any supervision. The results introduced involved four successful runs and one unsatisfactory run. Product from the micro-plant reactor were analysed from time to time by GC connected to the micro-plant until all the feed reactants have reacted. The success of the experimental runs was evaluated by the composition of TOME produced during the process. This was then followed by the reactive distillation results. Three runs of the latter were executed.

12.1 Micro-plant runs and results

The micro-plant runs were conducted using 0.50 dm^3 of feed. The pre-heater temperature and the reactor temperature of the reactor were varied between 60 °C, 70 °C and 80 °C. The feeds (TMP and methanol) were prepared with different percentage compositions. For instance; 50 mol-% of MeOH and 50 mol-% of TMP or 75 mol-% of MeOH and 25 mol-% of TMP. For the calculation of molar compositions; only methanol, TMP-I, TMP-2 and TOME were used in the computation. Impurities produced along with these compounds are not considered. The results of the runs are demonstrated below.

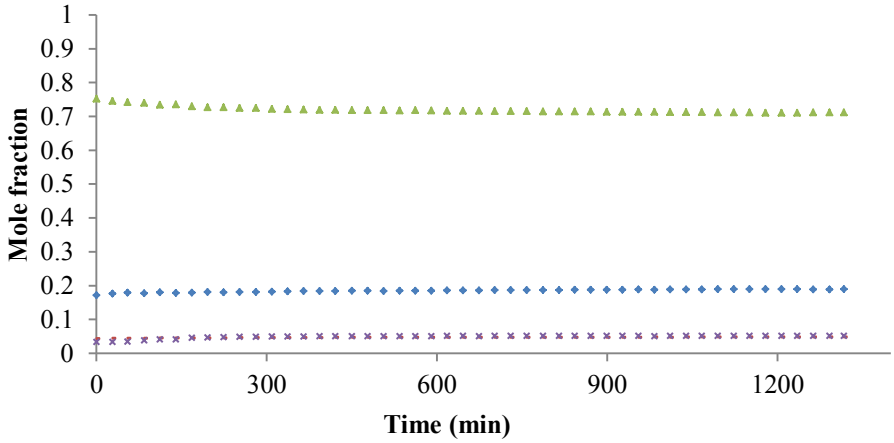

Figure 22: Micro-plant reactor run of 0.74 mole fraction MeOH and 0.26 mole fraction TMP feed at 60 °C. ◆, TMP-1; ■, TMP-2; ▲, MeOH; ×, TOME.

In Figure 22, 0.50 dm^3 feed contains 0.74 mole fraction of methanol and 0.26 mole fraction of diisobutylene. The operating condition for the reaction was 60 °C and 5.7 bar of nitrogen was introduced to pressurise the system, keeping the reaction in liquid phase. At equilibrium, mole fraction of product was 0.711 MeOH, 0.189 TMP-1, 0.047 TMP-2 and 0.051 TOME. The process lasted for 22 hours.

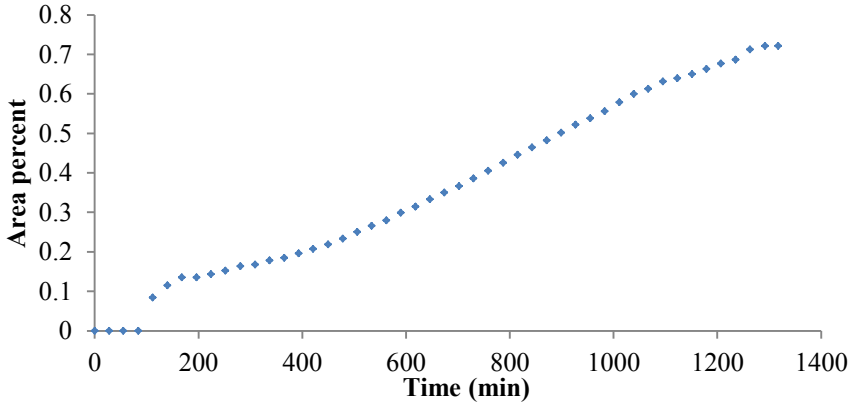

Figure 23: DME increase of 0.74 mole fraction MeOH and 0.26 mole fraction TMP feed at 60 °C. ◆, DME rise.

From Figure 23, the production of DME keeps increasing as the reaction progressed. At the end of the reaction, there was 0.72 mol-% of DME.

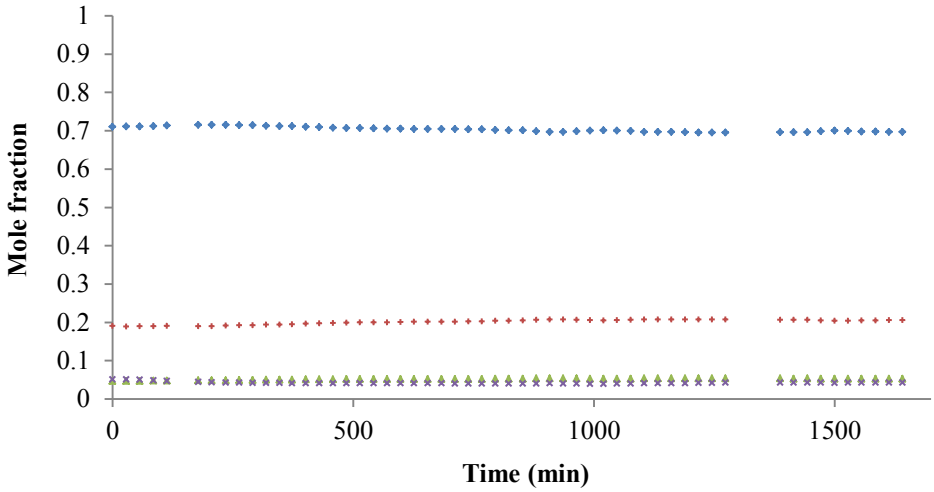

Figure 24: Micro-plant reactor run of 0.74 mole fraction MeOH and 0.26 mole fraction TMP feed at 70 °C. ◆, MeOH; +, TMP-1; ▲, TMP-2; ×, TOME.

In Figure 24, 0.5 dm^3 feed containing 0.74 mole fraction of methanol and 0.26 mole fraction of diisobutylene. The operating condition for the reaction was 70 °C and 6 bar of nitrogen was introduced to pressurise the system in order to keep the reaction in liquid phase. At equilibrium, the mole fraction of the product was 0.698 MeOH, 0.205 TMP-1, 0.053 TMP-2 and 0.043 of TOME. The reaction time was 28 hours.

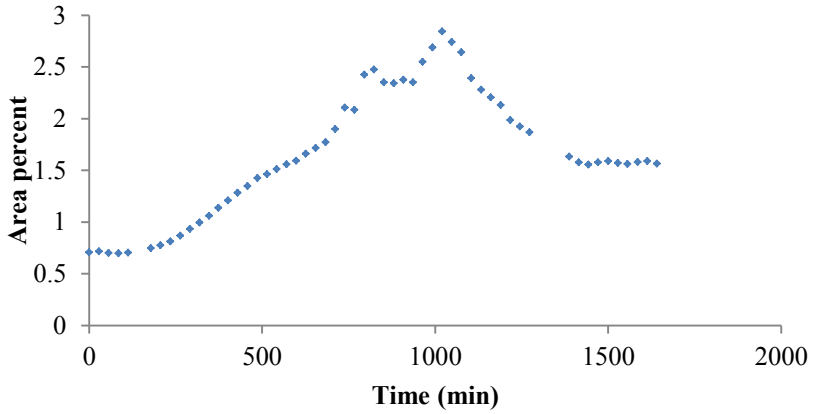

Figure 25: DME increase of 0.74 mole fraction MeOH and 0.26 mole fraction TMP feed at 70 °C. ◆, DME rise.

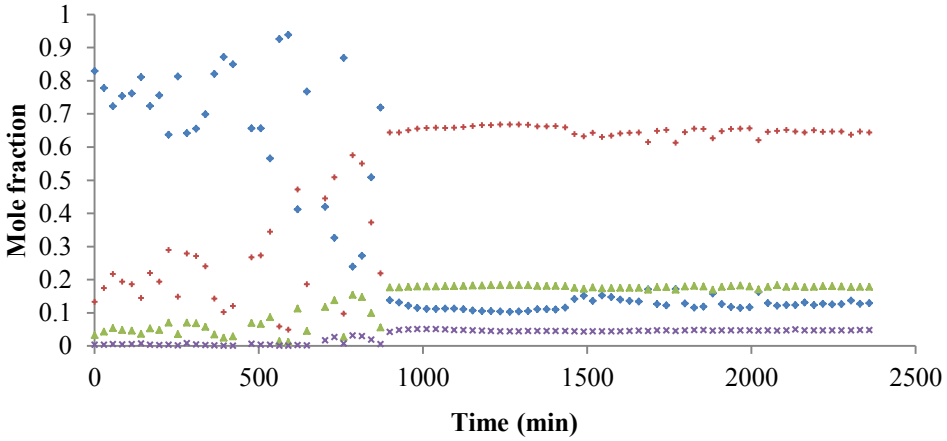

Figure 26: Micro-plant reactor run of 0.50 mole fraction MeOH and 0.50 mole fraction TMP feed at 80 °C. ◆, MeOH; +, TMP-1; ▲, TMP-2; ×, TOME.

In Figure 26, 0.50 dm^3 feed containing equimolar concentration of methanol and diisobutylene was utilised. The operating condition for the reaction was 80 °C and 6.3 bar of nitrogen was introduced to pressurise the system in order to keep the reaction in liquid phase. At the beginning of the process, there was so much nitrogen in the system. This resulted into instability of the process. When the nitrogen for the system was regulated, the reaction stabilised. At equilibrium, the mole fraction of the product was 0.127 MeOH, 0.647 TMP-1, 0.178-TMP-2 and 0.047 of TOME. The time of reaction was 40 hours.

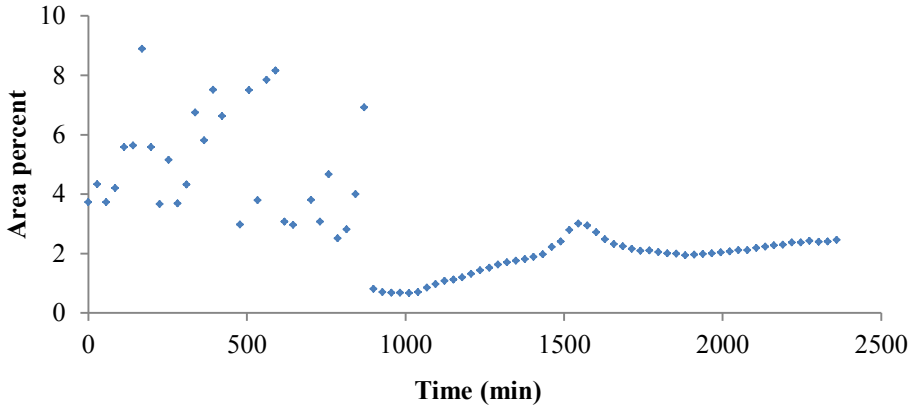

Figure 27: DME increase of 0.50 mole fraction MeOH and 0.50 mole fraction TMP feed at 80 °C. ◆, DME increase.

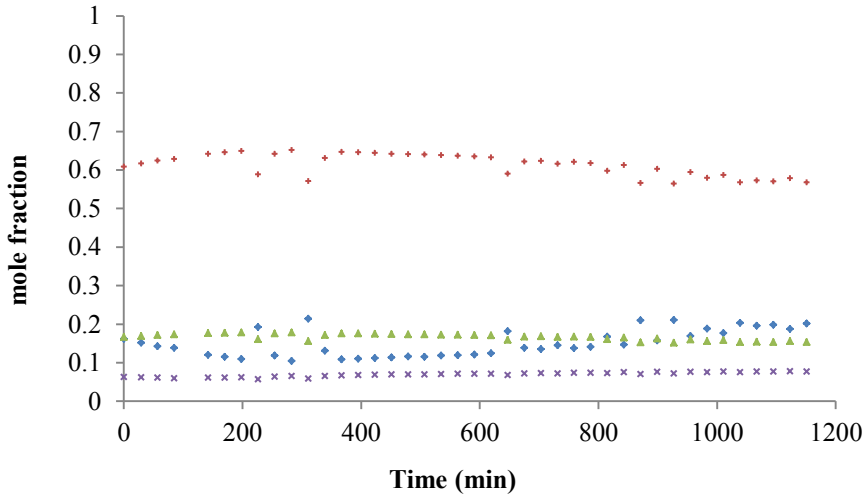

Figure 28: Micro-plant reactor run of 0.49 mole fraction MeOH and 0.51 mole fraction TMP feed at 70 °C. ◆, MeOH; +, TMP-1; ▲, TMP-2; ×, TOME.

In Figure 28, 0.50 dm^3 feed containing 49 mole percent of methanol and 51 mole percent of diisobutylene. The operating temperature was 70 °C and 4.8 bar of nitrogen was introduced to pressurise the system in order to keep the reaction in liquid phase. At equilibrium, the mole fraction of the product was 0.273 MeOH, 0.537 TMP-1, 0.142 TMP-2 and 0.078 of TOME

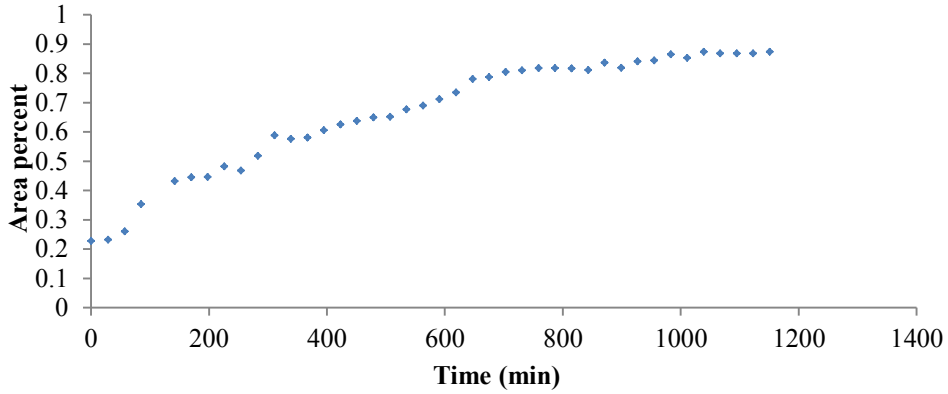

Figure 29: DME increase of 0.49 mole fraction MeOH and 0.51 mole fraction TMP feed at 70 °C. ◆, DME rise.

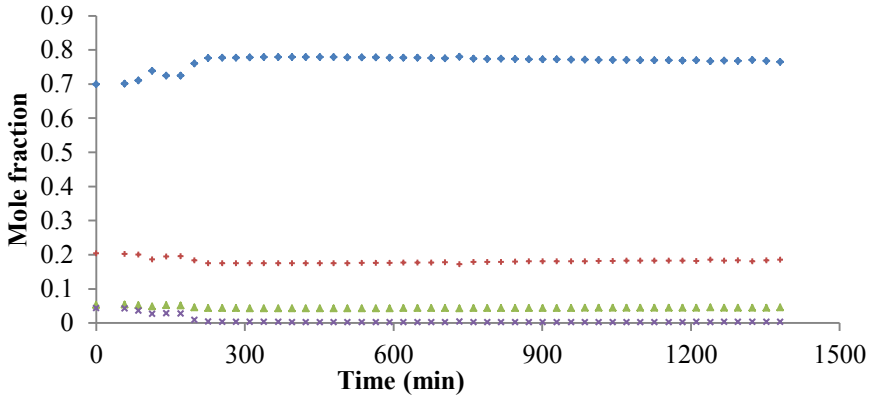

Figure 30: micro-plant reactor run of 0.75 mole fraction MeOH and 0.25 mole fraction TMP feed at 80 °C. ◆, MeOH; +, TMP-1; ▲, TMP-2; ×, TOME.

In Figure 30, 0.50 dm^3 feed containing 75 mole percent of methanol and 25 mole percent of diisobutylene was introduced into the reactor. The operating condition for the reaction was 80 °C and 6.9 bar of nitrogen was administered. After running the process for 141 minutes, the production of TOME declined. This might be due to leakage in the process. This represents an unsuccessful run.

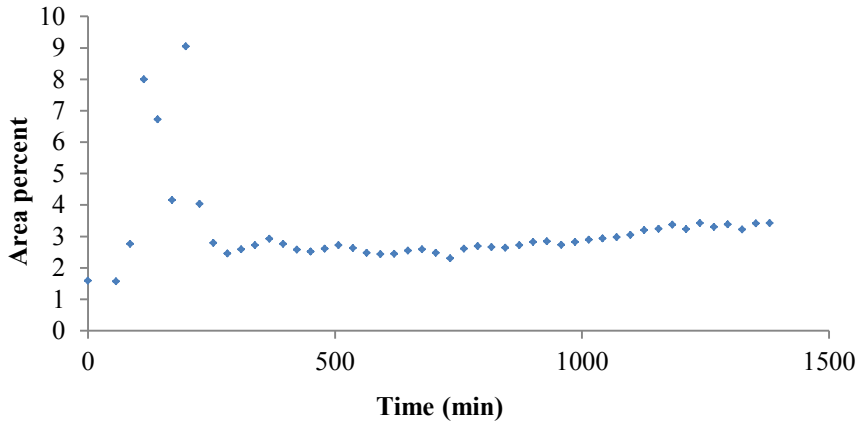

Figure 31: DME increase of 0.75 mole fraction MeOH and 0.25 mole fraction TMP feed at 80 °C. ◆, DME rise.

12.2 Reactive distillation runs and results

The temperature profile of the first run of RD is displayed below in figure 32. Three introductions of methanol were conducted. These points are visible on the temperature profile curve as the points where noticeable decline occur on the temperature measurement. The first introduction was executed when time was 92 minutes. After 4 hours of RD column run, the equipment was stopped and restarted the following day.

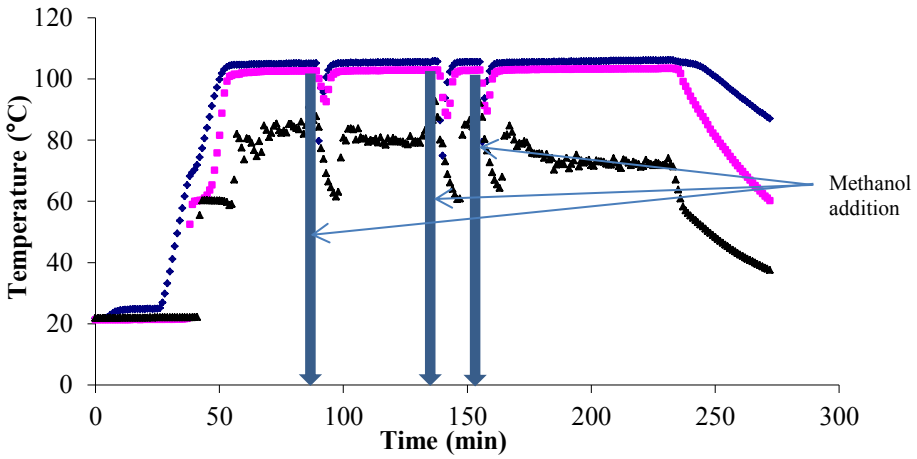

Figure 32: The temperature profile of first RD, Day 1 (27.08.2013). Three additions of methanol were conducted. ◆, temperature of bottom; ■, temperature of bottom of packed section; ▲, temperature of distillate.

Figure 33 shows the temperature profile when the process was restarted the next day. Only two additions of methanol were conducted. There was leakage of vapour from the system through the round bottom flask containing the bottom. The reactive distillation run was terminated. The error in this experimental run was then reviewed to prevent the recurrence of such mistake in subsequent RD runs.

In Figure 34, the conversion of methanol, TMP-1 and TMP-2 to TOME is demonstrated. In the last analysis conducted (from Table 8), after running the experiment for 5 hours, 13.7 mol-% of TOME, 63.1 mol-% of TMP-1, 23.5 mol-% of TMP-2 and 0 mol-% of methanol were present. There was however some impurities produced along with diisobutylene isomers in the bottom samples. Nonetheless, these impurities were not considered in the

molar percent computation because they are not compounds of interest in this research and their concentration level is very low.

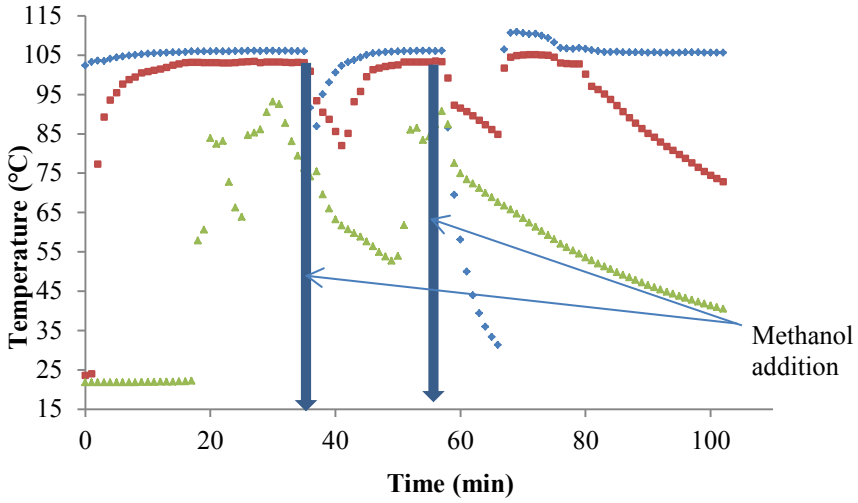

Figure 33: The temperature profile of first RD run, Day 2 (28.08.2013). ◆, temperature of bottom; ■, temperature of bottom of packed section; ▲, temperature of distillate.

Table 5: Area percent GC result of the last sample analysed for first RD.

Peak	Ret Time	Width	Area	Height	Area
#	[min]	[min]	[pA*s]	[pA]	%
1	0.22	0.00	908	2724	0.492
2	9.22	0.09	666	124	0.361
3	9.45	0.07	108000	21300	58.535
4	9.61	0.04	206	90	0.112
5	9.81	0.05	39600	10900	21.496
6	10.02	0.04	525	208	0.285
7	10.09	0.04	1271	490	0.690
8	10.30	0.04	331	138	0.179
9	10.64	0.04	417	163	0.226
10	11.22	0.03	1343	616	0.728
11	12.99	0.03	1556	768	0.844
12	13.31	0.03	157	78	0.085
13	13.85	0.04	25000	8162	13.546
14	14.49	0.06	3680	972	1.996
15	14.70	0.03	785	423	0.426

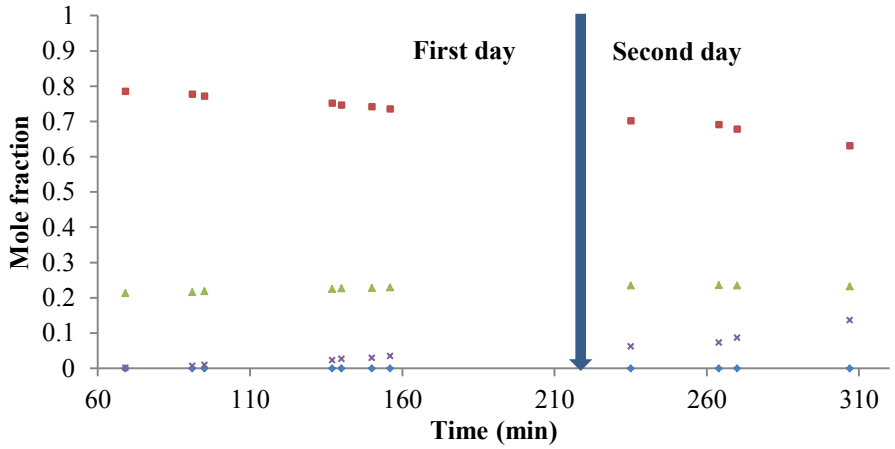

Figure 34: Composition of methanol, TMP-1, TMP-2 and TOME compositions in bottom samples analysed during first RD. computation. ◆, MeOH; ■, TMP-1; ▲, TMP-2; ×, TOME.

Figure 35 exhibits the compositions of distillates taken during the first RD run. However, distillate sampling at different intervals was not conducted for subsequent RD runs. This is because TOME is the chemical compound of interest which remains in the bottom. From the plot, methanol appeared in larger amount due to its low boiling point and VLE behaviour. TOME is hardly noticeable in the distillate because it is the heaviest component, so it is firmly attached to the bottom.

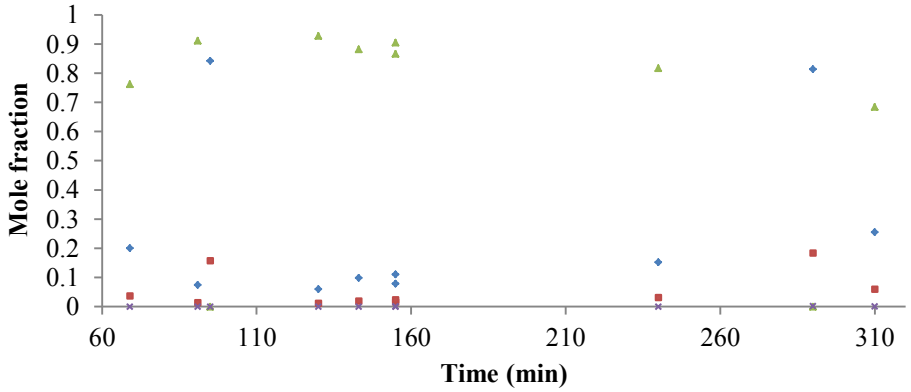

Figure 35: Composition of components in distillate for RD run 1. ◆, TMP-1; ■, TMP-2; ▲, MeOH; ×, TOME.

The second RD was executed for five days. The starting feed was composed of 525.99 g of diisobutylene and 7.89 g of methanol, 95.01 mol-% diisobutylene and 4.99 mol-% methanol. The first day of run was executed for 5 hours 50 minutes with the concentration of the last bottom sample analysed being 7.83 mol-% of TOME. When the process was continued the next day, the operating time was 9 hours. The last bottom sample investigated was 25.94 mol-% of TOME. On the third day, the operating time was 5 hours. The concentration of the last bottom sample analysed improved from 25.94 mol-% to 33.06 mol-% of TOME. The only bottom sample examined on the fourth day of experimental run contains 37.27 mol-% of TOME after 5 hours. On the last day, after 7 hours 42 minutes, the bottom composition was 0 mol-% methanol, 30.91 mol-% TMP-1, 12.50 mol-% TMP-2 and 56.60 mol-% TOME.

The temperature profiles of the experimental run are displayed below. In addition, conversions of the reactants for TOME production are also portrayed.

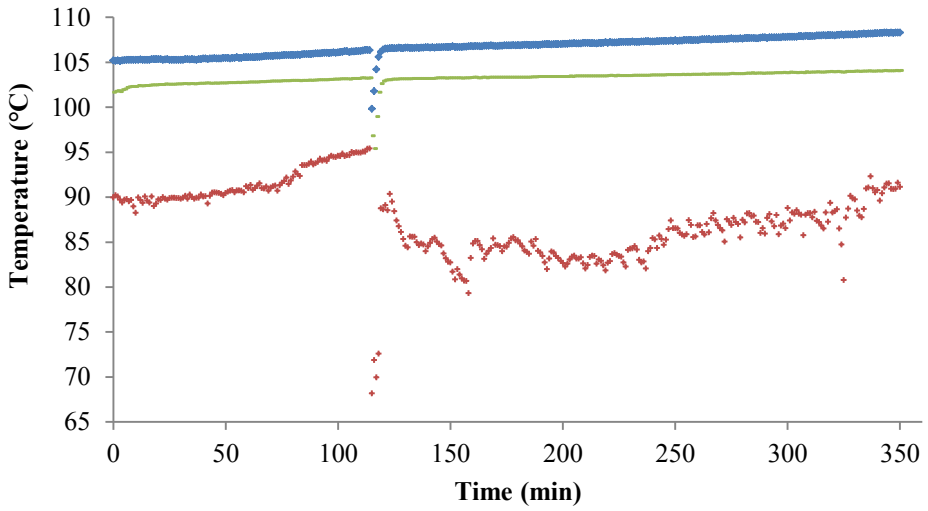

Figure 36: The temperature profile of day 1 (12.09.2013) of second RD run. ◆, bottom; +, distillate; -, bottom of packed column.

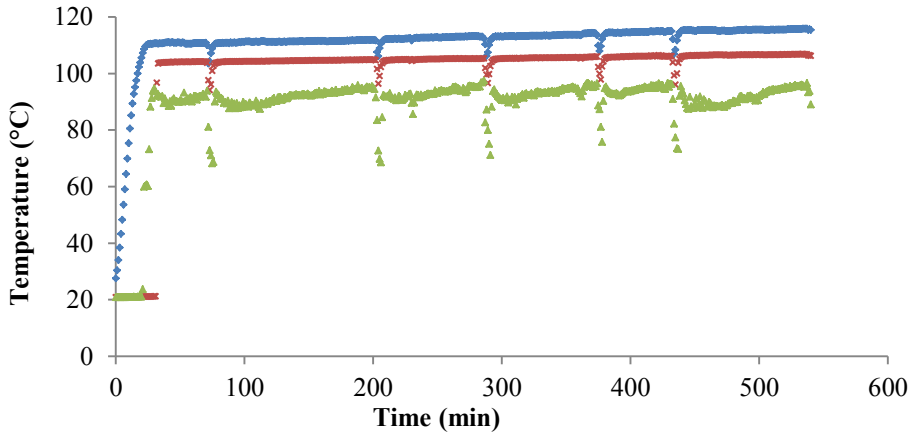

Figure 37: The temperature profile of second RD run, day 2 (13.09.2013). ◆, temperature of bottom; ■, temperature of bottom of packed section; ▲, temperature of distillate.

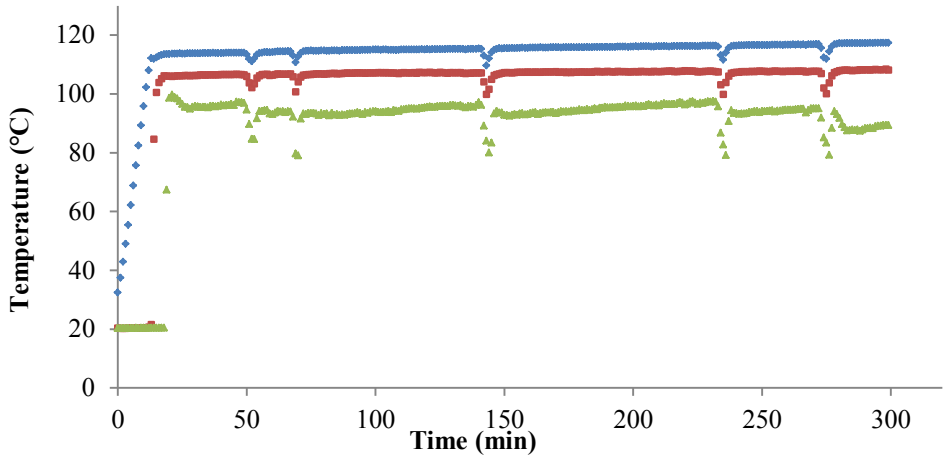

Figure 38: Temperature profile of second RD run day 3 (16.09.2013). ◆, temperature of bottom; ■, temperature of bottom of packed section; ▲, temperature of distillate.

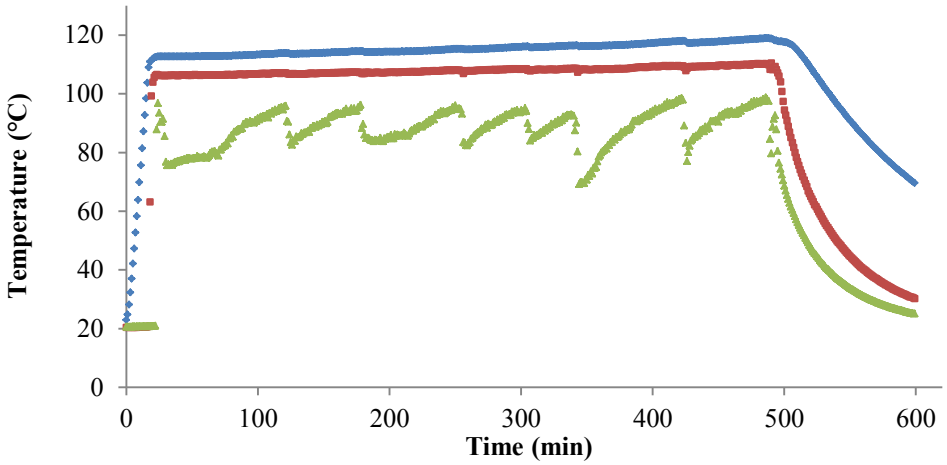

Figure 39: The temperature profile of day 4 (23.09.2013) of second RD run. ◆, bottom; ■, bottom of packed column; ▲, distillate.

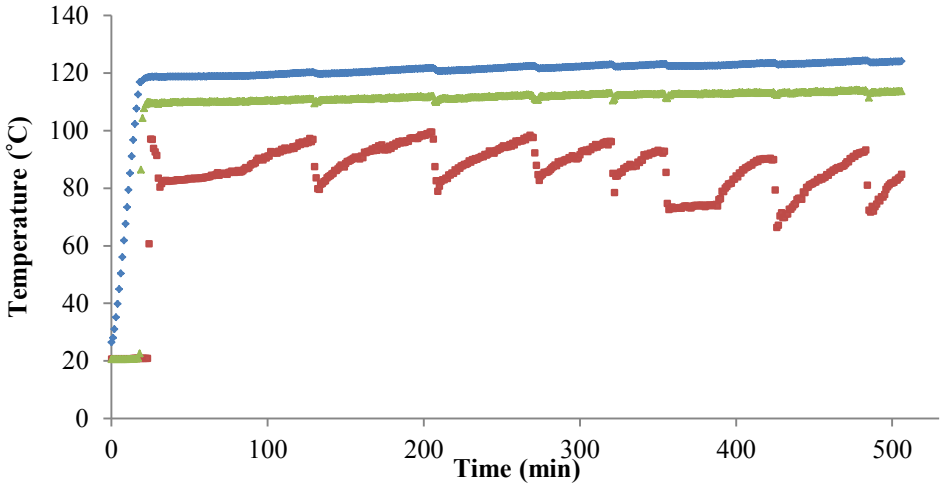

Figure 40: The temperature profile of day 5 (24.09.2013) of second RD run. ◆, bottom; ■, distillate; ▲, bottom of packed column.

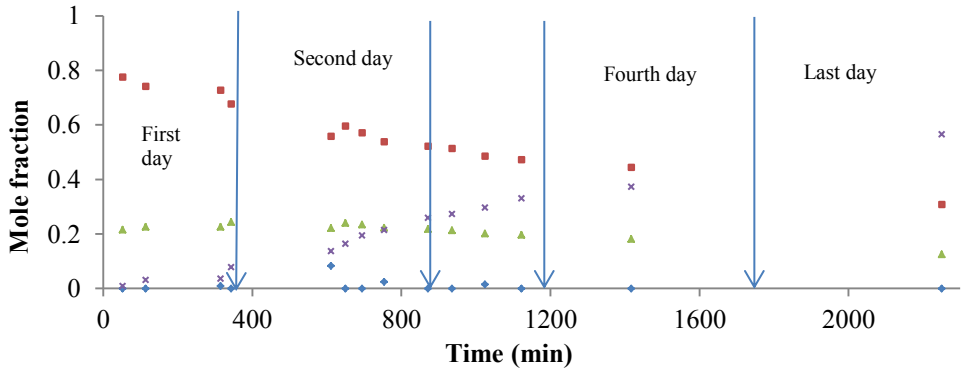

Figure 41: Composition of samples examined during second RD. ◆, MeOH; ■, TMP-1; ▲, TMP-2; ×, TOME.

In Figure 42, the temperature profile of the bottom and distillate is demonstrated. The bottom temperature augmented from 105.41 °C to 123.36 °C. The temperature of the distillate fluctuates. This is because addition of methanol to the system decreases the operating temperature of the column. However, the reduction of temperature is more conspicuous on the temperature profile of distillate as earlier demonstrated by Figure 36 to Figure 40. The temperature of the bottom and distillate is a function of the methanol, TMP-1, TMP-2 and TOME composition. At the start of the experiment when there is no TOME, the temperature is low. As TOME is being produced in the bottom, the temperature rises.

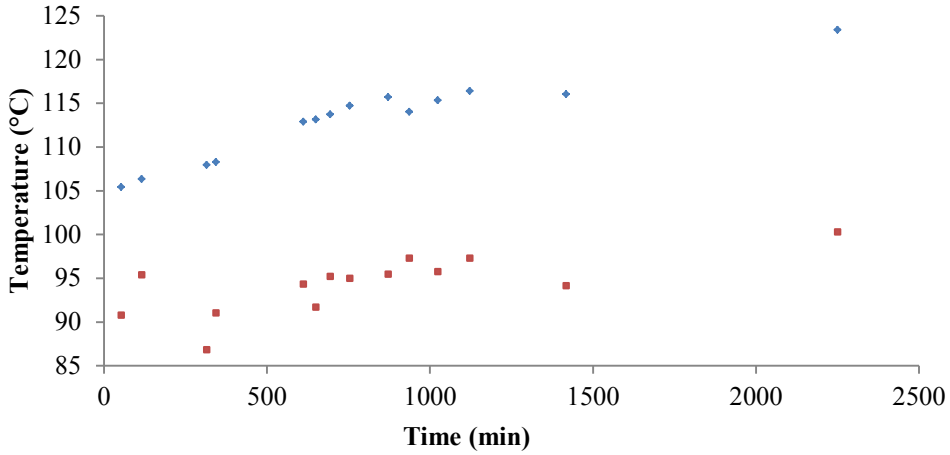

Figure 42: The temperature profile of the bottom and distillate sections during the progress of second RD run. ◆, bottom; ■, distillate. The time displayed in the figure is the summation of operating period for each day.

After the successful production of TOME in second RD, the main focus of the third RD run centers around computation of the mass balance of this process. The catalyst used for this run was also Amberlyst catalyst utilised in first and second RD runs. This RD was conducted for 10 days. The first day lasted for 4 hours and 14 minutes with the last sample analysed on this day containing only 2.77 mol-% TOME. The second day was conducted for 293 min, last sample investigated being 11.12 mol-% TOME. The third day was executed for 590 minutes with the last sample examined being 14.81 mol-% TOME. The fourth, fifth, sixth, seventh, eighth, ninth and last day terminated after 426 minutes, 506 minutes, 503 minutes, 299 minutes, 348 minutes, 545 minutes and 33 minutes respectively. On the ninth day, at the

end of the run, the composition of the bottom was 0 mol-% methanol, 22.10 mol-% TMP-1, 8.11 mol-% TMP-2 and 69.78 mol-% TOME. On the last day, when the first sample analysed comprised of 5.12 mol-% methanol, 24.37 mol-% TMP-1, 8.49 mol-% TMP-2 and 62.02 mol-% TOME, it was decided to top the process. This is a decline from the preceding day from 69.78 mol-% TOME to 62.02 mol-% TOME.

For the mass balance calculation, 710.12 g of diisobutylene and 10.50 g of methanol were utilised as the feed. There were subsequent additions of methanol when the methanol in the column is consumed. Due to the side reaction of the decomposition of methanol to form water and dimethyl ether, water was withdrawn from the distillate from time to time. The organic phase is returned back to the column (mainly methanol and diisobutylene). This is visible from the liquid-liquid split in the distillate. The aggregate mass of methanol used for the third RD run was 270.29 g. At the end of the third RD run, 199.13 g of water phase was removed from the system with 501.15 g of bottom sample retained in the round bottom flask. The composition of the water phase when analysed by GC was 86.29 mol-% MeOH, 9.08 mol-% of TMP-1 and 4.62 mol-% water. The bottom sample was further purified. From the molar composition of the water phase, the actual dimethyl ether formed during the experiment was computed.

Table 6: Mass balance for third RD run.

Molar mass (g/mol)	MeOH	DME	Water	TMP-1
	32.04	46.07	18.0153	112.21
Mass of water phase (g)	199.1300			
Mole fraction of water	0.0462			
Mole fraction Methanol	0.8629			
Mol fraction of TMP-1	0.0908			
Mass of water (g)	0.8330			
Mass of Methanol (g)	27.6496			
Mass of TMP-1 (g)	10.1928			
Total mass of water, TMP-1 and Methanol	38.6755			
Mass composition of water in water phase	4.2891	g		
Mass composition of methanol in water phase	142.3606	g		
Mass composition of TMP-1 in water phase	52.4803	g		
Number of moles of water in water phase	0.2381	mol		
Number of moles of methanol in water phase	4.4430	mol		
Number of moles of TMP-1 in water phase	0.4677	mol		
Mass of DME lost through condenser	10.9684	g		
Mass of diisobutylene used as feed	710.1200	g		
Mass of bottom	501.1500	g		
Mass of samples taken for analysis	70.00	g		
Mass of methanol used during run	270.2900	g		
Mass of organic phase in bottle	22.6700	g		
Mass introduced into the column	980.4100	g		
Mass out of column	803.9184	g		
Error in mass balance	176.49	g		

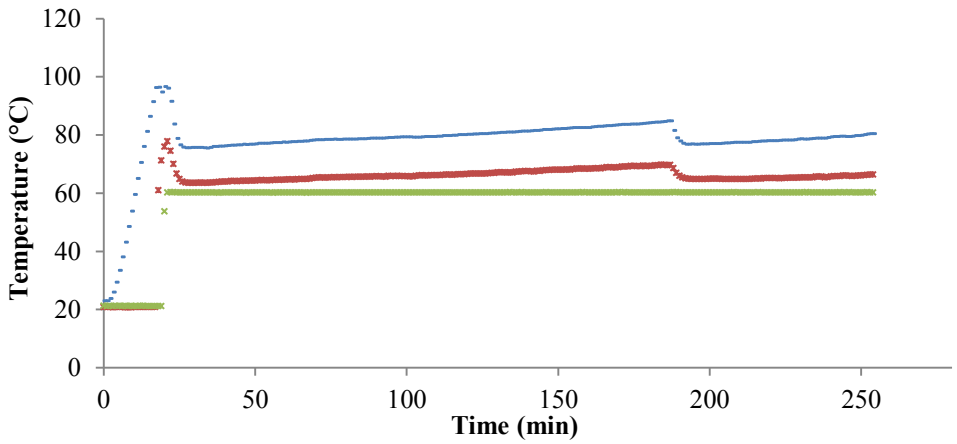

Figure 43: Temperature profile of third RD, day 1 (18.9.2013). ▪, bottom; ✳, bottom of packed section; ×, distillate.

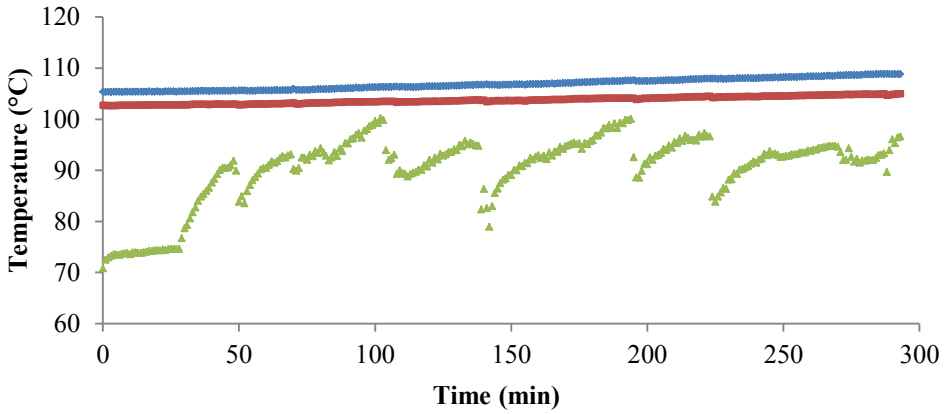

Figure 44: The temperature profile third RD, day 2 (19.09.2013). ◆, bottom; ■, bottom of packed section; ▲, distillate.

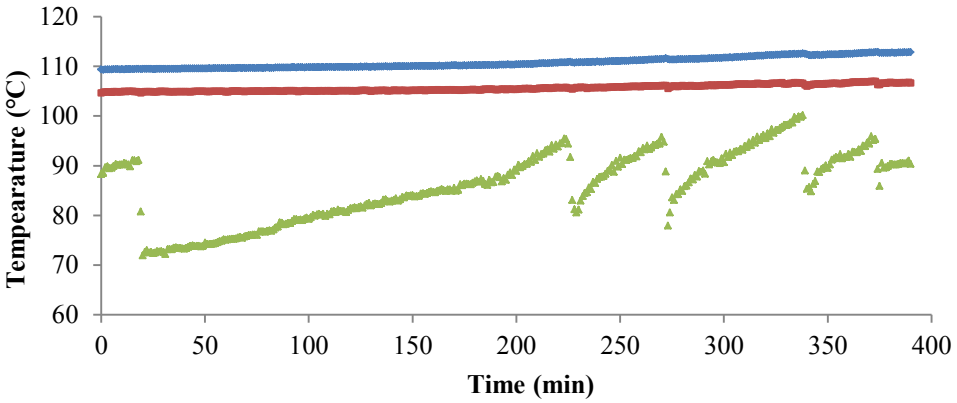

Figure 45: The temperature profile of third RD run , day 3 (20.09.2013). ◆, bottom; ■, bottom of packed section; ▲, distillate.

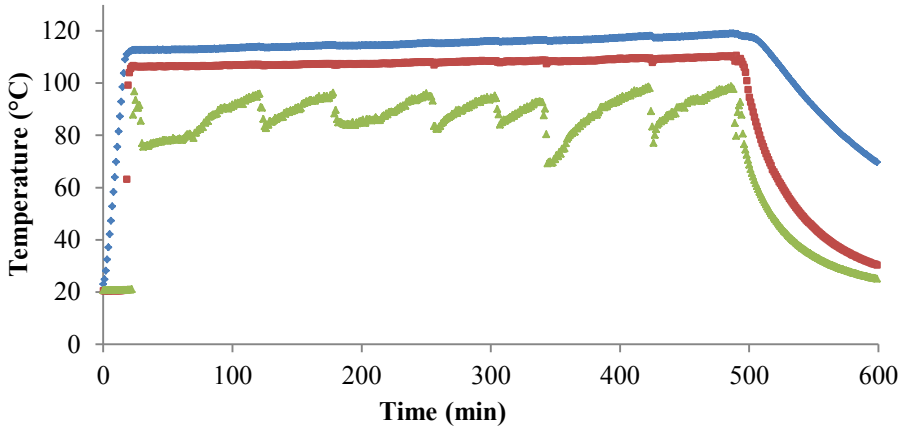

Figure 46: The temperature profile of third RD run, day 4. ◆, bottom; ■, bottom of packed section; ▲, distillate.

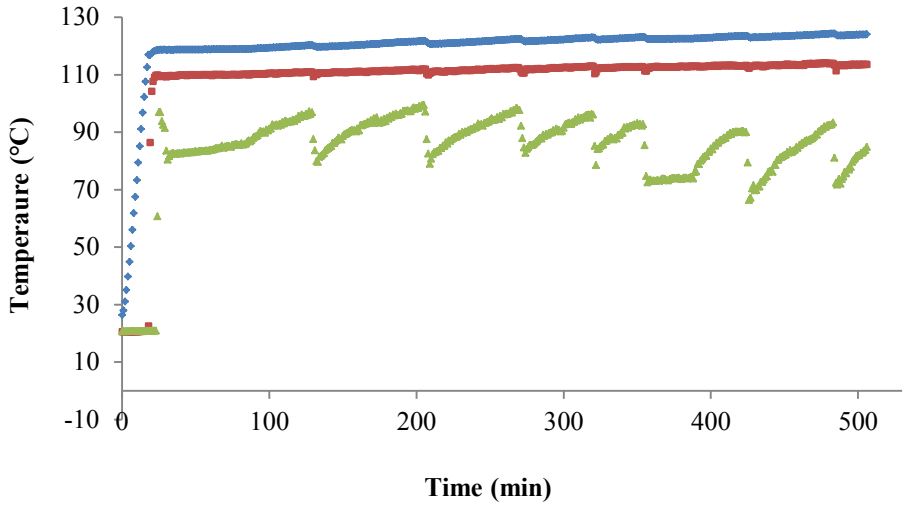

Figure 47: The temperature profile of third RD run, day 5 (24.09.2013). ◆, bottom; ■, distillate; ▲, bottom of packed column.

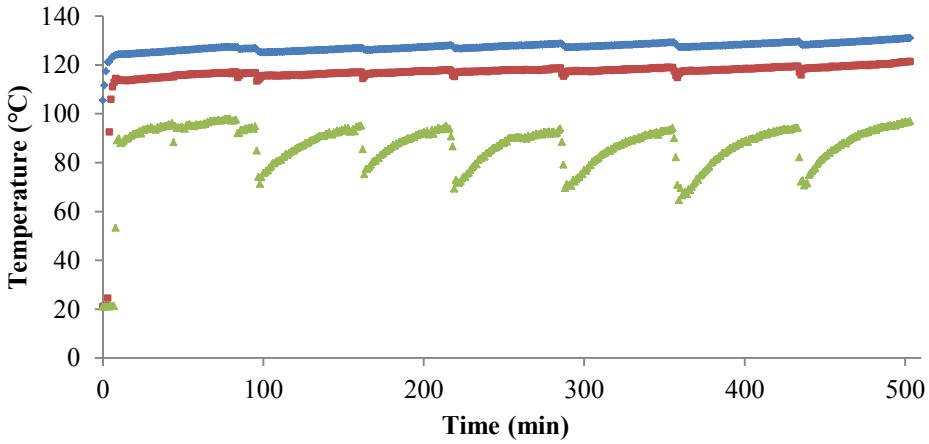

Figure 48: The temperature profile of third RD run, day 6 (25.09.2013). ◆, bottom; ■, distillate; ▲, bottom of packed column.

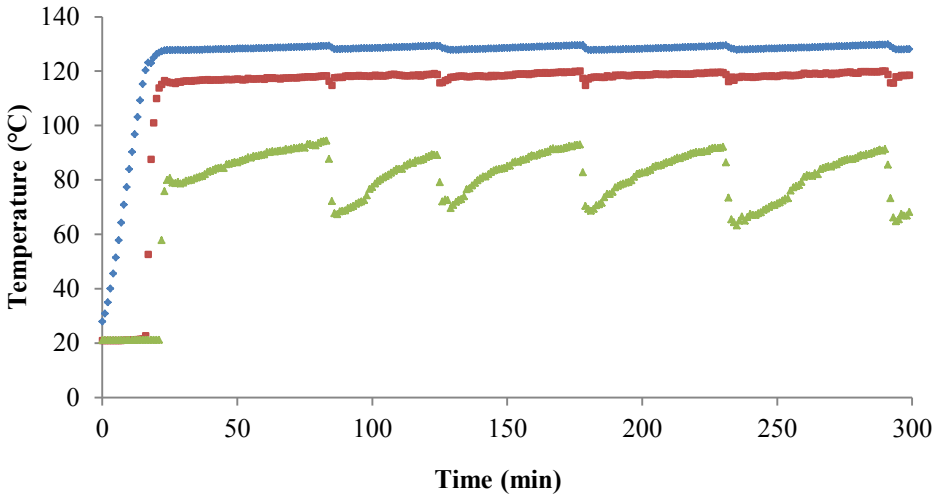

Figure 49: The temperature of third RD run, day 7 (26.09.2013). ◆, bottom; ■, bottom of packed section; ▲, distillate.

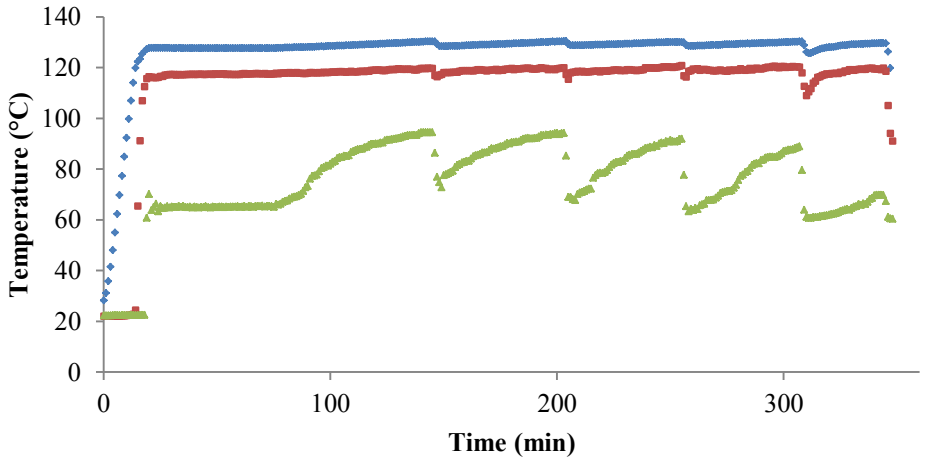

Figure 50: The temperature of third RD run, day 8 (27.09.2013). ◆, bottom; ■, bottom of packed section; ▲, distillate.

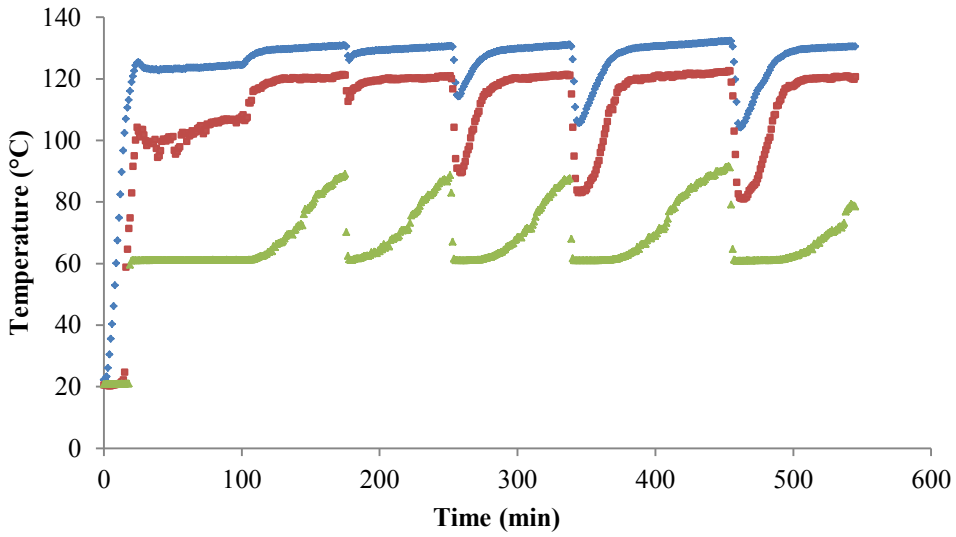

Figure 51: The temperature profile of third RD run, day 9 (30.09.2013). ◆, bottom; ■, bottom of packed section; ▲, distillate.

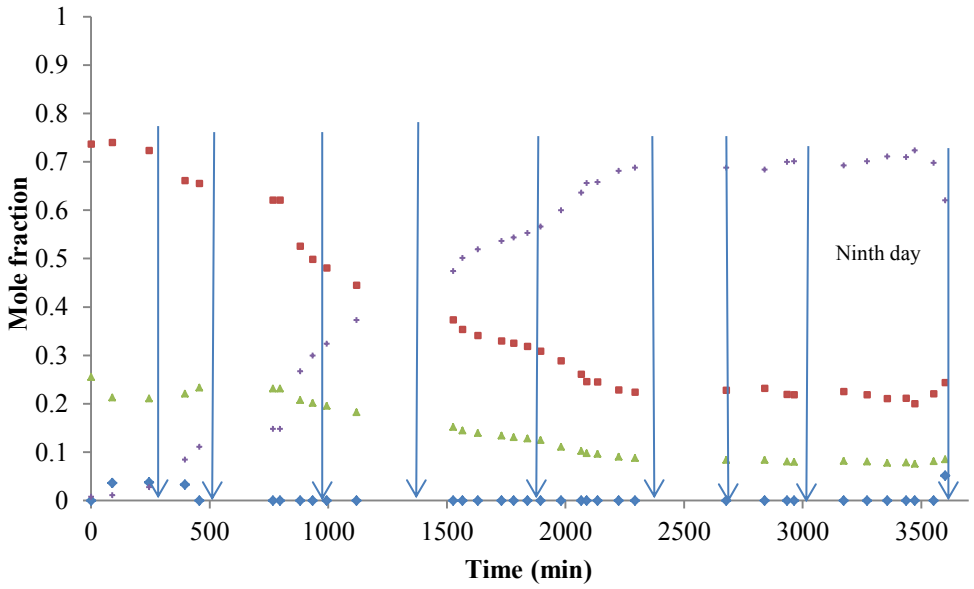

Figure 52: Composition of methanol, TMP-1, TMP-2 and TOME in bottom samples analysed during the course of third RD run. ◆, MeOH; ■, TMP-1; ▲, TMP-2; +, TOME.

13. Separation processes implemented after experimental runs

In the micro-plant runs, after the production of impure TOME, distillation was first employed. Subsequently, liquid-liquid extraction was utilised. Water was added to the fractions after distillation in a conical flask. However, there were droplets of liquid phase in organic phase and vice versa. The conical flask was then implanted in an ultrasonic bath to achieve distinct liquid phase and organic phase. The purity level of the highest fraction accomplished after purification was composed of 96 mol-% TOME. On the contrary, after the RD runs, distillation and rotavapor were employed for purification.

The same distillation column utilised for RD was modified (removal of catalytic section) for distillation after the second RD run. The packed section was composed of 6 mm x 6 mm “Assistent” raschig ring of clear glass. After the distillation, rotavapor was applied to obtain higher purity level of TOME. The fraction to be purified is introduced to the round bottom flask labelled “D” in Figure 53. The heating bath is initiated. Once the boiling point of each component of the flask is attained, boiling occurs. The vapour is condensed and collected as liquid in the round bottom flask labelled “C”. After some rotavapor runs, the bottom of the last run when analysed by GC resulted into 98.01 mole percent TOME.

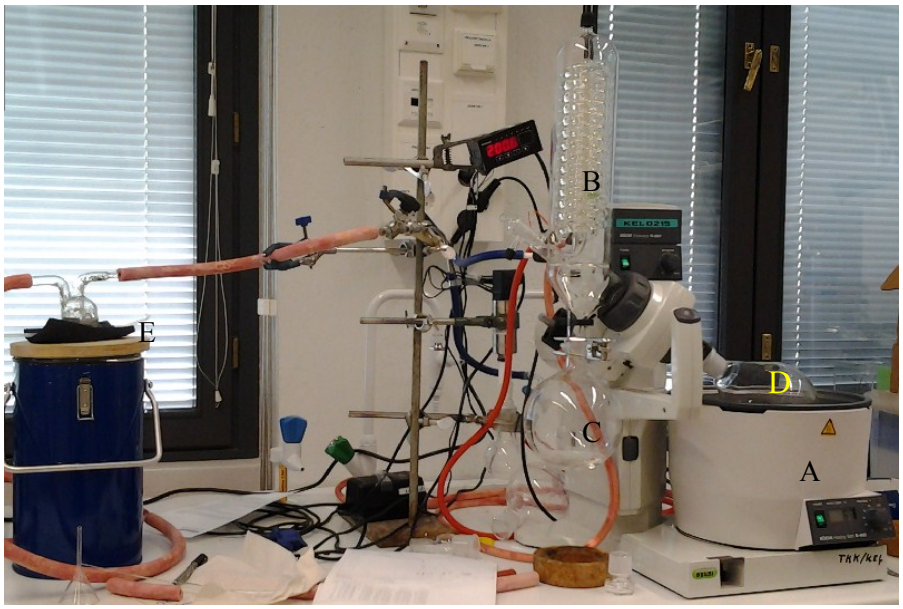

Figure 53: The Büchi rotavapor R-200 implemented after second RD run. A; heating bath, B; condenser, C; distillate, D; bottom, E, vacuum. The operation of the rotavapor was vacuum-assisted through the red pipes.

After the third RD run, composed of 5 mol-% methanol, 24 mol-% TMP-1, 8 mol-% TMP-2 and 62 mol-% TOME, the same RD column was employed for conventional distillation. Different fractions were collected as distillate and later analysed by GC. The fractions comprised of high concentration of TOME were combined in one conical flask. The aggregate concentration was later analysed as: 0.027 mole fraction of methanol, 0.381 mole fraction of TMP-1, 0.142 mole fraction of TMP-2 and 0.450 mole fraction of TOME. This was further purified by another distillation column (Figure 54) having a narrow column. The column diameter is 2.4 cm and length of the column is 95 cm. After some successive collections of distillate from the top of the column, the last bottom sample analysed by GC comprised of 99.05 mole percent of TOME. Fortunately, there were no traces of methanol, TMP-1 and TMP-2.

The 98.01 mole-% TOME produced after the implementation of rotavapor on second RD run was also subjected to this distillation column. The purity level was improved to 99 mole percent TOME. This narrow column produced the best result for the purification of TOME. However, the two significant drawbacks of this column are; the heat loss in the column is high

and at elevated input power of the reboiler, flooding occurs. Low input power does not elevate vapour to the top of the column.

The heat loss issue was resolved by applying insulation to the column. The second problem of the column (flooding) was solved by first utilising high input power before flooding occurs. When the temperature in the column is gradually increasing, the power is then decreased. This resulted into prevention of flooding and raises the vapour in the column. Consequently, there was collection of distillate.

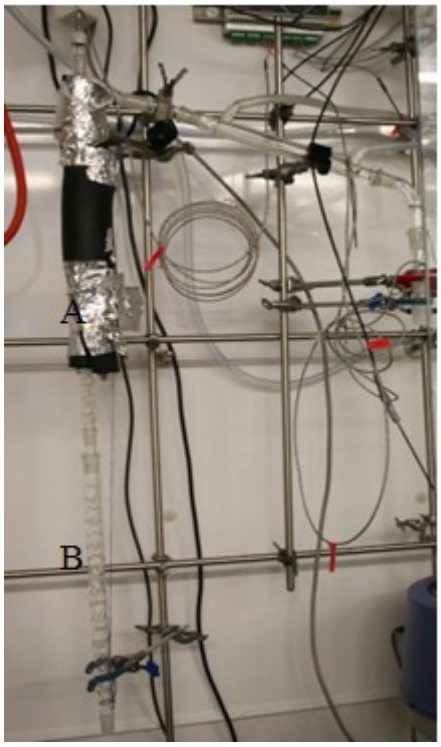

Figure 54: The narrow distillation column utilised. A, insulation. The insulation at part labeled “B” was displaced in order to have a good view of the column.

14. Physical property measurement

After the production of TOME in this research, some of the physical properties of the ether will be determined. The other physical properties of interest, such as liquid-liquid equilibrium measurement, will be resolved as a continuation of this project in future by Aalto chemical engineering research group.

The only physical property which was ascertained after the production of 99.05 mole percent TOME was density measurement. Though, the density measurement was not executed immediately because the only measurement of TOME accessible in literature was conducted at 25 °C. Nonetheless, prior to the measurement, the density of 98.90 mole percent 2,4,4-trimethyl-1-pentene (TMP-1) was investigated.

The density meter available, DMA 5000 M density meter by Anton Paar, could determine density between 20 °C to 95 °C. After the determination of the density of TMP-1 by this equipment, the values were compared with literature data to assess this device. Figures 55 and 56 depict the measurement.

Table 7: Comparison of the density measurement of TMP-1 with the periodic time obtained for density determination on calibration data. ^{lit}, Danner and Daubert; ^{meas}, this work.

T (°C)	T (K)	ρ^{lit} (kmol/m^3)	ρ^{lit} (g/cm^3)	ρ^{meas} (g/cm^3)	Periodic time (µs)	Absolute Error
20	293.15	6.3722	0.7150	0.7156	3366.47	-0.0005
25	298.15	6.3346	0.7108	0.7114	3363.14	-0.0006
30	303.15	6.2967	0.7066	0.7072	3354.72	-0.0007
35	308.15	6.2584	0.7023	0.7030	3348.25	-0.0007
40	313.15	6.2199	0.6980	0.6988	3347.81	-0.0008
45	318.15	6.1810	0.6936	0.6932	3342.56	0.0004
50	323.15	6.1418	0.6892	0.6887	3337.03	0.0005
55	328.15	6.1022	0.6847	0.6843	3331.76	0.0005
60	333.15	6.0623	0.6803	0.6814	3326.47	-0.0011

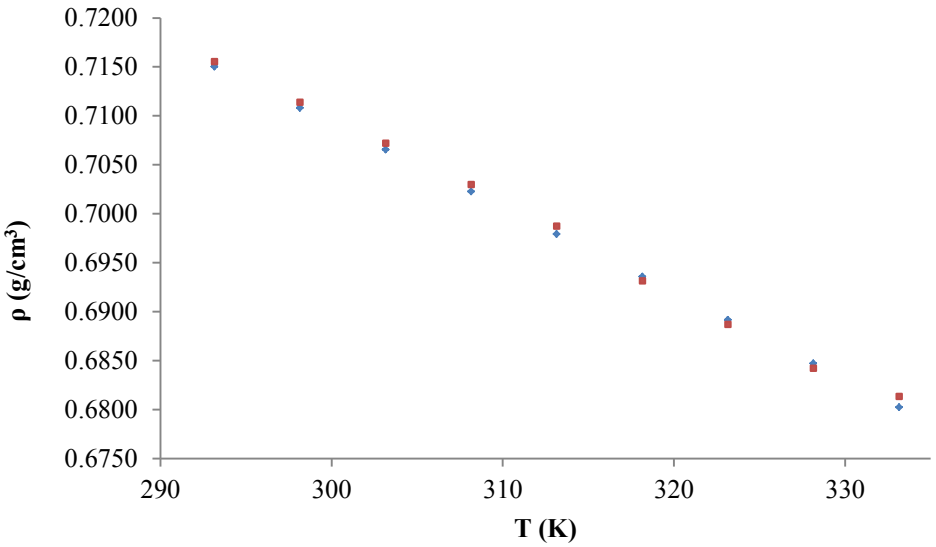

Figure 55: Density measurement of 98.9 mole percent TMP-1. ■, density measurement in this work; ◆, Danner and Daubert.

From Figure 55, although the DMA 5000 densimeter has the capacity to measure density up to 368.15 K, however the boiling point of TMP-1 (374.59 K) is being approached. As a result, the TMP-1 sample in the equipment is about boiling, preventing accurate measurement above 60 °C. In order to measure unerring density above 333 K with this apparatus, the solvent needs to be degassed.

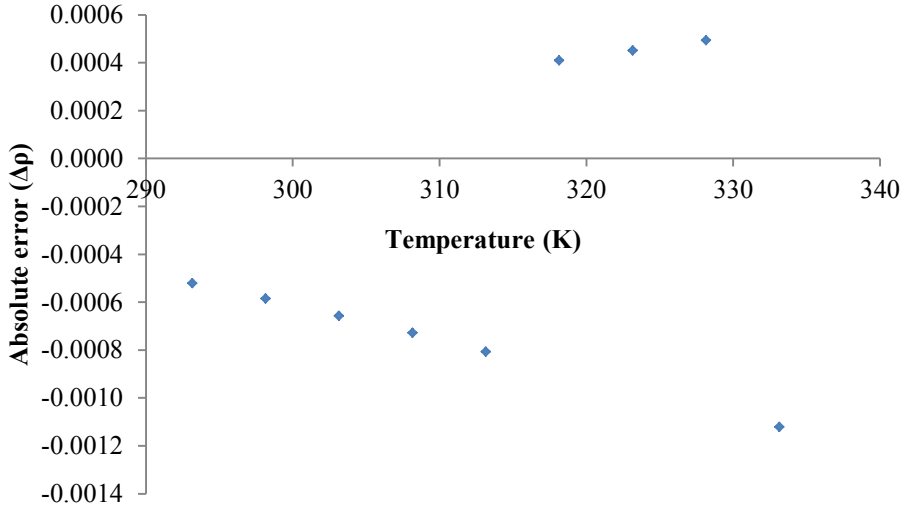

Figure 56: Error in density measurement of TMP-1 between measured and literature values. ◆, Error.

Absolute error, $\Delta\rho = \rho^{meas} - \rho^{lit}$

For TOME density measurement, the sample was injected with the syringe through the point laballed “A” in Figure 57. After the injection, the equipment displays if there is presence of bubbles on the screen through the oscillating U-tube sensor on the screen. The bubbles are withdrawn by injecting more samples until the screen exhibits the absence of bubbles on the oscillating U-tube sensor. Through the screen, the unit for density measurement, the desired temperature for the density measurement could be inputted and altered for subsequent measurements.

Figure 57: DMA 5000 M density meter used for density measurement. The point A is the sample introduction point.

In Uusi-Kyyny et al. (2001), density measurement of TOME was conducted at 298.15 K by Anton-Paar-40 vibrating tube densimeter. Nevertheless, the TOME manufactured in this research is of higher purity. In this thesis, the density of TOME was ascertained at 293.15 K to 358.15 K. The oscillation period and the estimated density value of the equipment at each temperature were recorded. The oscillation periods were inserted into recently prepared calibration data for this equipment. The analysis result is presented below in Table 8.

Table 8: Density measurement of 99.05 mole percent TOME analysed by GC. At 25 °C, the measured value in this research was compared with that in Uusi-Kyyny et al. (2001).

T/ °C	T/K	Period time (µs)	ρ^{meas} (g/cm^3)	ρ^{Lit} (g/cm^3)
20	293.15	3471.87	0.7986	
25	298.15	3466.87	0.7946	0.7930
30	303.15	3461.84	0.7905	
35	308.15	3456.80	0.7864	
40	313.15	3451.76	0.7823	
45	318.15	3446.71	0.7782	
50	323.15	3441.65	0.7740	
55	328.15	3436.58	0.7698	
60	333.15	3431.49	0.7656	
65	338.15	3426.38	0.7613	
70	343.15	3421.25	0.757	
75	348.15	3416.13	0.7526	
80	353.15	3410.99	0.7482	
85	358.15	3405.82	0.7438	
90	363.15	3400.12	0.73880	
95	368.15	3394.95	0.7343	
At 298.15 K, the error in density measurement of TOME was -0.0016 g/cm^3				

A model was developed with Microsoft excel for the measured density between 20 °C to 95 °C (Appendix VII)**.** Density parameter values of TMP-1 and MTBE in DIPPR 801 database were utilised to predict the initial guess values for TOME parameters (A, B, C and D). The sum of relative errors was used as the objective function and optimised to zero. The correlation employed for the density modeling is displayed below:

$$\rho = \frac{A}{B^{[1+(1-T/C)^D]}}$$

Table 9: The correlation parameters and the recommended temperature range for the measured density of TOME.

Component	**2-methoxy-2,4,4-trimethylpentane**
A	0.1687
B	0.4159
C	500.0020
D	0.2941
T_{min} (K)	293.15
T_{max} (K)	368.15

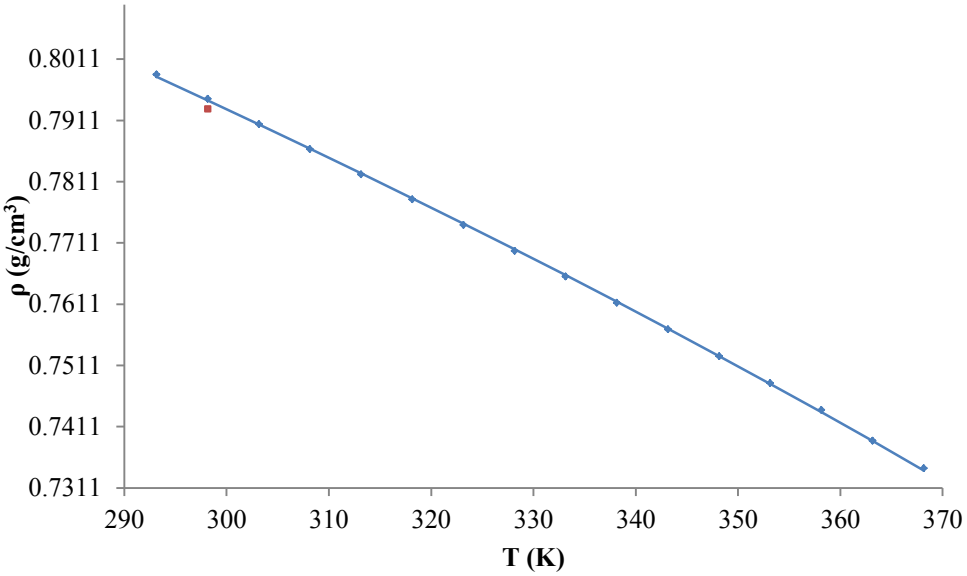

Figure 58: TOME density measurement. ◆, this research; ■, Uusi-Kyyny et al. and —, model at 298.15 K. Data in (Appendix VII).

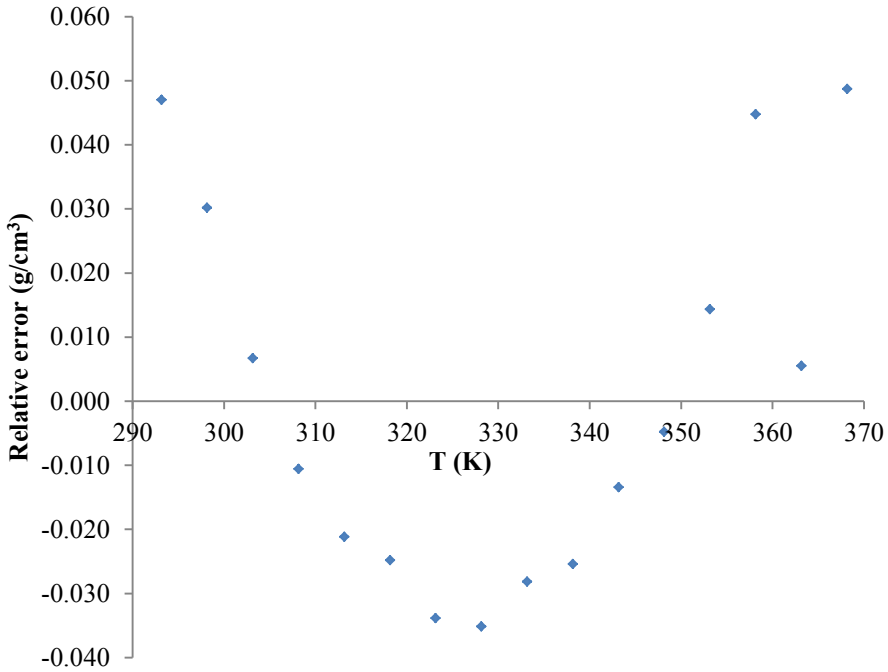

Figure 59: Absolute error of TOME density between the measured and model values. ◆; absolute error.

15. Discussion and conclusions

2-methoxy-2,4,4-trimethylpentane (TOME) has been identified as a fuel oxygenate capable of substituting MTBE as fuel additive. Fuel oxygenates help improve the octane rating of gasoline and prevent engine from knocking. Presently, production of TOME is not feasible on commercial scale. The aim of this thesis was to produce the chemical with a high purity percentage on laboratory scale by implementing a micro-plant unit. In addition to the micro-plant, reactive distillation was employed to compare the effectiveness of these two techniques.

TOME production is generally a slow process as observed in the micro-plant reactor and reactive distillation runs. Each micro-plant reactor run was conducted for over 20 hours with the highest purity of TOME produced being just 5 mol-%. For some of the reactor runs, obtaining the high pressure required to keep the reaction in liquid phase was challenging. Operation of the micro-plant entails a vast expertise of chemical and plant design proficiencies.

In contrast to the micro-plant runs, operation of the reactive distillation runs was less tedious. After the initiation of the process, the essential task required for successful run is the inspection of the operating temperature of the distillate to detect if methanol addition should be administered. The other task is the procurement of bottom samples for gas chromatography analysis.

Generally, the implementation of RD distillation generated TOME of higher purity and the conversion of the reactants have been immensely improved than in micro-plant reactor runs. Consequently, time required for separation processes after the runs have also been greatly influenced. The improvement on TOME purity in the bottom by RD is an encouraging achievement considering the cost and time required for separation.

Reactive distillation has a great potential of improving the quality and yield of various processes. The conversion rate of the reactants in the second RD run was 56 %. In the third RD run, the conversion rate was over 70 % at a

time but later retrogressed to 62 % due to the decomposition of TOME and the formation of heavier compounds. RD has been selected over micro-plant for future production of TOME.

16. Recommendation for future research

In the current research, execution of the RD experiment at temperature of about 80 °C increased the rate of reaction, though water phase formed in the distillate has a higher composition than when operating at 90 °C. So it is advisable to control the experiment at temperature region of 80 °C. Likewise, the rate of TOME production at the beginning of each reactive distillation run was very fast. However, when over 40 mol-% of TOME has been manufactured in the bottom, it requires more than one hour in obtaining a molar percent increment in TOME production in some cases.

Moreover, the absence of methanol in the RD column for a long period of time will result to the formation of oligomers, occurring as impurities for this process. This will prevent proper production of TOME even if additional methanol is introduced into the RD column.

After the initiation of the process, there might be the introduction of pump which could inject methanol into the column continuously in cm^3 volume. This will help abolish the stress encountered during methanol injection into the system at regular interval.

The mass balance discrepancy (176.49 g) observed in third RD caused by leakage in the process shows that there is still room to improve the mass balance accuracy of this equipment in subsequent RD experiments. Before the inception of future RD runs, all the connection points in the RD apparatus must be properly investigated to avoid leakage during runs.

References

Adeosun, J.T., Lawal, A., *Numerical and experimental studies of mixing characteristics in a T-junction microchannel using residence-time distribution,* Chemical Engineering Science **64** (10) (2009) 2422–2432.

Adeosun, J.T., Lawal, A., *Residence-time distribution as a measure of mixing in T-junction and multilaminated/elongational flow micromixers,* Chemical Engineering Science **65** (5) (2010) 1865–1874.

Angelescu, D.E., Mercier, B., Siess, D., Schroeder, R., *Microfluidic capillary separation and real-time spectroscopic analysis of specific components from multiphase mixtures*, Anal. Chem. **82** (2010) 2412–2420.

Arora, A., Simone, G., Salieb-Beugelaar, G.B., Kim, J.T., Manz, A., *Latest developments in micro total analysis systems*, Anal. Chem. **82** (2010) 4830–4847.

Barrow, D.A., Castell, O.K., Sykes, N., Myers, Ritchie, P.H., *A microfabricated graphitic carbon column for high performance liquid chromatography*, J. Chromatogr. A. **1218** (2011) 1983–1987.

Boyd, D.A., Adleman, J.R., Goodwin, D.G., Psaltis, D., *Chemical separations by bubble-assisted interphase mass-transfer*, *Anal. Chem*., **80** (2008) 2452–2456.

Calabrese, G.S., Pissavini, S., *From batch to continuous flow processing in chemicals manufacturing*, AIChE J. **57** (2011) 828–834.

Danner, R.P. Daubert, T.E. Technical Data Book-Petroleum Refining, 5th Edition American Petroleum Institute, Washington, D.C. 1992-extant.

Davis, G., *Executive order D-5-99 by the Governor of the State of California*, 25 March 1999.

Doherty, M., Buzad, G., *Reactive distillation by design*, Chem. Eng. Res. Des. **70** (1992) 448-458.

Dörhöfer, T., *Gestaltungund Effektivit von Bodenkolonnen für die Reaktivrektifikation*, Ph.D. Thesis, Technische Universität, München 2006.

EFOA, *European Ether Market and Outlook, 2010,* http://www.efoa.eu/en/markets.aspx, Accessed on August 9th, 2013.

Ehrfeld, W., Hessel, V., Möbius, H., Russow, K., *Potential and realization of microreactors*, In: Ehrfeld, W. (Ed.), Microsystem Technology for Chemical and Biological Microreactors, 1996, DECHEMA-Monographs Mainz. pp. 1–2.

von Harbou, E., Schmitt, M., Hasse, H., *Morphological analysis for the development of reliable models for heterogeneously catalysed reactive distillation*, Chemical Engineering Science **91** (2013) 134–145.

Fanelli, M., Arora, R., Glass, R., Litt, D., Silva, L., Tonkovich, A.L., and Weidert, D., *Comput. Methods Multiphase Flow* **56** (2007) 205–213.

Fink, H. and Hampe, M.J., *Designing and constructing microplants, in IMRET 3*, Ehrfeld, W. (ed) (Springer-Verlag, Berlin, Germany) 2000, pp. 664–673.

Gmehling J., Kolbe, B., Kleiber, M., Rarey, J., Chemical thermodynamics for process simulation, 2012, 735 p.

Götze, L., Bailer, O., Moritz, P., von Scala, C., *Reactive distillation with KATAPAK (R)*, Catal. Today **69** (2001) 201–208.

Gress, D., Hartmann, H., Kaibel, G. and Seid, B., *Use of mathematical simulation and miniplant techniques in process development*, Chem.-hzg.-Tech., **51** (1979) 601-606, 611.

Grob, R.L.; Barry, E.F.; Modern practice of gas chromatography, John Fourth edition, Wiley & sons, inc, Publication, 2004, pp 285-286.

Hartman, R.L., Jensen, K.F., *Microchemical systems for continuous-flow synthesis*, Lab. Chip **9** (2009) 2495–2507.

Hartman, R.L., Sahoo, H.R., Yen, B.C., and Jensen, K.F., *Distillation in micro-chemical systems using capillary forces and segmented flow*, Lab Chip **9** (2009) 1843–1849.

Hessel, V., Hardt, S., Löwe, H., *Micro Chemical Process Engineering*, Wiley-VCH, Weinheim, 2004.

Hessel, V., Löb, P., Krtschil, U., Löwe, H., *Microstructured reactors for development and production in pharmaceutical and fine chemistry*, in: Ernst Schering Foundation Symp. 3, Berlin, 2007, 205–240.

Hibara, A., Toshin, K., Tsukahara, T., Mawatari, K., and Kitamori, T., *Microfluidic Distillation Utilizing Micro-Nano Combined Structure*, Chem. Lett. 37 (2008) 1064–1065.

Jamaguchi, T., J. Tokyo Chem. Soc. **34** (1913) 691.

Karinen, R., *Doctoral thesis: Etherification of some C8-alkenes to fuel ethers*, Helsinki University of Technology, Espoo, 2002.

Karinen, R., Krause, O., *Reactivity of some C8-alkenes in etherification with methanol*, Appl. Catal. A **188** (1999) 247-256.

Kistenmacher, H., Personal communication, 1995.

Kockmann, N., Gottsponer, M., Roberge, D.M., *Scale-up concept of single-channel microreactors from process development to industrial production*, Chem. Eng. J. **167** (2011) 718–726.

Krishna, R., *Reactive separations: more ways to skin a cat*, Chem. Eng. Sci. **57** (2002) 1491-1504.

Krishna, R., 2003, *Hardware selection and design aspects for reactive distillation columns*. In: Sundmacher, K., Kienle, A. (Eds.), Reactive Distillation. Wiley- VCH, Germany, pp. 169–189.

Kuhn, S., Noel, T., Gu, L., Heider, P.L., Jensen K.F., *A Teflon microreactor with integrated piezoelectric actuator to handle solid forming reactions*, Lab. Chip **11** (2011) 2488–2492.

Kulikov, D.; Verevkin, S. P.; Heintz, A., *Determination of vaporization enthalpies of the aliphatic branched C5 and C6 alcohols from transpiration method*, J. Chem. Eng. Data **46** (2001)[a] 1593-1600.

Kulikov, D.; Verevkin, S. P.; Heintz, A., *Enthalpies of vaporization of a series of linear aliphatic alcohols. Experimental results and predicted values using the ERAS-model*, Fluid Phase Equilib. **192** (2001)[b] 187-207.

Kyaw, T., Fujiwara, T., Inoue, H., Okamoto, Y., Kumamaru, *Reversed micellar mediated luminol chemiluminescence detection of iron(II, III) combined with on-line solvent extraction using 8-Quinolinol*, T., Anal. Sci. **14** (1998) 203.

Luyben, W., L., *Distillation design and control using Aspen^{TM} simulation*, John Wiley & Sons, Inc., Hoboken, New Jersey, **2006**, pp. 232-235.

Luyben, W., L., *Design and control of the methoxy-methyl-heptane process*, Ind. Eng. Chem. Res. **49** (2010) 6164–6175.

MacInnes, J.M., Ortiz–Osorio, J., Jordan, P.J., Priestman, G.H., Allen, R.W.K., *Experimental Demonstration of Rotating Spiral Microcha nnel Distillation,* Chem. Eng. J., **159** (2010) 159–169.

Maier, S. and Kaibel, O., *Scale-down of chemical engineering pilot plant - what is attainable*? Chem..hlg.-Teeh,, **62** (1990) 169-174.

Malone, M.F., Doherty, M.F., *Reactive distillation*, Ind. Eng. Chem. Res. **39** (2000) 3953-3957.

Mawatari, K, Kazoe, Y., Aota, A,, Tsukahara, T., Sato, K., Kitamori, T., *Microflow systems for chemical synthesis and analysis: approaches to full integration of chemical process*, J. Flow Chem. **1** (2011) 3–12.

Müller, A., Cominos, V., Hessel, V., Horn, B., Schürer, J., Ziogas, A., Jähnisch, K., Hillmann, V., Großer, V., Jam, K.A., Bazzanella, A., Rinke, G., Kraut, M., *Fluidic bus system for chemical process engineering in the laboratory and for small-scale production*, Chemical Engineering Journal, **107** (1–3) (2005) 205-214.

Müller, D., Minh, D.H., Merchan, V.A., Arellano-Garcia, H., Kasaka, Y., Müller, M., Schomäker, R., and Wozny, G., *Towards a novel process concept for the hydroformylation of higher alkenes: Mini-plant operation*

strategies via model development and optimal experimental design, Chemical Engineering Science 2013.

Papachristos, M.J., Swithenbank, J., Priestman, G.H., Stournas, S., Polysis, P., Lois, E., *Effects of the molecular structure of anti-knock additives on engine performance*, Journal of the Institute of Energy **64** (1991) 113-123.

Pedro A. Robles, Teófilo A. Graber, Martín Aznar, *Prediction by the ASOG method of liquid–liquid equilibrium for binary and ternary systems containing 1-alkyl-3-methylimidazolium hexafluorophosphate*, Fluid Phase Equilibria **287** (2009) 43-49.

Piel, W.J., *Dimerization reaction of isobutene*, Fuel reformulation **4** (2) (1994) 28-33.

Perry J.A., *Introduction to analytical gas chromatography*: *History, principles and practice*, Marcel Dekker, New York, 1981.

Raal**,** J.D**.,** Mühlbauer**,** A.L**.,** Phase Equilibria: Measurement and Computation, Taylor & Francis, Bristol, PA, 1998.

Ramirez-Gonzalez, E.A., Martinez, C. and Alvarez, J., *Modeling zero-gravity distillation*. Ind. Eng. Chem. Res., **31** (3) (1992) 901–908.

Rihko, L.K., Krause, A.O.I., *Etherification of FCC light gasoline with methanol*, Ind. Eng. Chem. Res., **35** (8) (1996) 2500-2507.

Roberge, D.M., Zimmermann, B., Rainone, F., Gottsponer, M., Eyholzer, M., Kockmann, N., *Microreactor technology and continuous processes in the fine chemical and pharmaceutical industry: Is the revolution underway?,* Org. Process Res. Dev. **12** (2008) 905–910.

Robbins, L.A., *Pilot plant operations - the miniplant concept*, Chem. Eng. Prog., **75** (1979) 45-48.

Sameshima, J., J. Am. Chem. Soc. **40** (1918) 1483.

Sandler, S.I., and Orbey, H., *Modeling Vapor-liquid equilibria; Cubic equation of state and their mixing rules*, Cambridge University Press, New York, 1998, pp. 5-7.

Schmitt, M., von Harbou, E., Parada, S., Grossmann, C., Hasse, H., *New equipment for laboratory studies of heterogeneously catalyzed reactive distillation*, Chem. Eng. Technol. **32** (2009) 1313–1317.

Seok, D.R. and Hwang, S., *Zero-gravity distillation utilizing the heat pipe principle (micro-distillation)*, AIChE J., **31** (12) (1985) 2059–2065.

Silva, L.,Weidert, D., Litt, R., Tonkovich, A.L., Arora, R. and Fanelli, M., *Exergetic efficient distillation in microchannel architecture,* AIChE Spring Meeting, April 2007.

Sloan, D., Birkhoff, R., Gilbert, M., Nurminen, M., Pyhälahti, A., *Isooctane Production from C4's as an Alternative to MTBE*, National Petrochemical & Refiners Association Paper AM-00-34, NPRA, Washington D.C. 2000.

Sotowa, K.I. and Kusakabe, K., *Proc. 4th ECCE Conf*., Granada, Spain 2003.

Sotowa, K.I. and Kusakabe, K., *IMRET 7*, Lausanne, Switzerland 2003.

Struckmann, L.K., Karinen, R.S., Krause, A.O.I., Jakobsson, K., Aittamaa, J.R., *Process configurations for the production of the 2-methoxy-2,4,4-trimethylpentane - a novel gasoline oxygenate*, Chemical engineering and Processing **43** (2004) 57-65.

Sundberg, A., Uusi-Kyyny, P., and Alopaeus, V., *Novel micro-distillation column for process development*, Chemical engineering research and design **87** (2009) 705-710.

Sundberg A.T., Uusi-Kyyny P., Alopaeus V., *Microscale distillation*, Russian Journal of general chemistry **82** (12) (2012),

Tonkovich, A.L., Simmons, W.W., Silva, L.J., Qiu, D., Perry, S.T., Yuschak, T., Hickey, T.P., Arora, R., Smith, A., Litt, R.D., and Neagle, P., US Patent 7610775 B2, 2009.

Tschernjaew, J., Kenig, E. and Górak, A., *Mikrodestillation von mehrkomponentensystemen,* Chem. Ing. Tech., **68** (3) (1996) 272–276.

Uusi-Kyyny, P.,* Pokki, J-P, Aittamaa, J., and Liukkonen, S., *Vapor-Liquid Equilibrium for the Binary Systems of Methanol + 2,4,4-Trimethyl-1-pentene at 331 K and 101 kPa and Methanol + 2-Methoxy-2,4,4-trimethylpentane at 333 K,* J. Chem. Eng. Data **46** (2001) 1244-1248.

Verevkin, S.P., Krasnykh, E.L., Vasiltsova, T.V., Heintz, A., *Determination of ambient temperature vapor pressures and vaporization enthalpies of branched ethers*, J. Chem. Eng. **48** (2003) 591-599.

Verevkin, S. P.; Wandschneider, D.; Heintz, A., *Determination of vaporization enthalpies of selected linear and branched C7, C8, C9, C11, and C12 monoolefin hydrocarbons from transpiration and correlation gas-chromatography methods*, J. Chem. Eng. *Data* **45** (2000) 618-625.

Wörz, O., *Process development via a miniplant*, Chem. Eng. Process **34** (1995) 261–268.

Zhang, T., Datta, R., *Ethers from ethanol-5. Equilibria and kinetics of the coupled reaction network of 3-methyl-3-ethoxypentane synthesis*, Chem. Eng. Sci. **51** (4) (1996) 649-661.

Ziogas, A., Cominos, V., Kolb, G., Kost, H.J., Werner, B., Hessel, V., *Development of a microrectification apparatus for analytical and preparative applications*, Chem. Eng. Technol. **35** (2012) 58–71.

APPENDIX 1

VLE Data (measured liquid-phase mole fraction (x_1) and measured vapour-phase mole fractions (y_1), temperature (T) and pressure (P) and activity coefficients for methanol (1)-2,4,4-trimethylpentene (2) system (Uusi-Kyyny et al., 2001).

x_1	y_1	T (K)	P (kPa)	$\gamma 1$	$\gamma 2$
1.000	1.000	337.35	100.2	1.00	
0.9869	0.9385	336.16	100.9	1.00	15.51
0.9764	0.9042	335.37	100.9	1.01	13.79
0.9632	0.8718	334.67	100.9	1.01	12.12
0.9351	0.8297	333.76	100.9	1.03	9.43
0.8503	0.7833	333.06	101.0	1.10	5.33
0.7997	0.7752	332.99	101.0	1.16	4.14
0.6793	0.7659	333.01	101.0	1.35	2.69
0.6103	0.7629	333.07	101.0	1.49	2.24
0.5489	0.7614	333.12	101.0	1.65	1.94
0.4751	0.7577	333.22	101.0	1.89	1.69
0.4198	0.7568	333.32	101.0	2.13	1.53
0.3619	0.7517	333.43	101.0	2.44	1.41
0.3002	0.7503	333.61	100.9	2.91	1.29
0.2450	0.7481	333.92	100.9	3.52	1.19
0.1995	0.741	334.29	100.9	4.22	1.14
0.1438	0.7301	335.14	100.9	5.57	1.08
0.0950	0.7075	336.99	100.9	7.61	1.03
0.0642	0.6817	339.05	100.9	10.02	1.01
0.0514	0.6599	341.06	100.9	11.22	0.99
0.0399	0.6192	343.76	100.9	12.27	1.00
0.0311	0.5689	347.66	100.9	12.54	0.99
0.0218	0.5024	351.47	100.8	13.79	1.00
0	0	374.15	100.7		1.00

APPENDIX II

The bottom and distillate temperatures, mole fractions of methanol, TMP-1, TMP-2 and TOME when bottom samples (B) were analysed on GC during first reactive distillation run.

Sample	Time (min)	Bottom T (°C)	Distillate T (°C)	nMEOH	nTMP-1	nTMP-2	nTOME
B1	69	104.91	83.94	0	0.786	0.213	0.001
B2	91	97.11	77.36	0	0.777	0.216	0.007
B3	95	104.18	100.31	0	0.772	0.218	0.010
B4	137	105.57	79.51	0	0.753	0.225	0.023
B5	140	105.89	92.71	0	0.747	0.226	0.027
B6	150	102.28	66.15	0	0.742	0.228	0.030
B7	156	105.62	92.16	0	0.736	0.230	0.035
B8	235	105.65	63.85	0	0.703	0.235	0.063
B9	264	106.08	90.42	0	0.692	0.236	0.073
B10	270	105.94	76.33	0	0.678	0.235	0.086
B11	307	110.38	61.35	0	0.631	0.232	0.137

APPENDIX III

The bottom and distillate operating temperature, mole fractions of methanol, TMP-1, TMP-2 and TOME of bottoms analysed during second reactive distillation run.

Sample	Time (min)	Bottom T (°C)	Distillate T (°C)	nMEOH	nTMP-1	nTMP-2	nTOME
B1	52	105.41	90.77	0	0.776	0.215	0.009
B2	115	106.32	95.38	0	0.742	0.226	0.031
B3	315	107.95	86.81	0.01	0.728	0.226	0.036
B4	343	108.28	91.04	0	0.677	0.245	0.078
B5	611	112.87	94.32	0.08	0.558	0.222	0.137
B6	650	113.13	91.68	0	0.596	0.240	0.164
B7	694	113.72	95.19	0	0.571	0.234	0.195
B8	754	114.71	94.99	0.02	0.539	0.223	0.214
B9	871	115.70	95.46	0.00	0.523	0.218	0.259
B10	936	114.01	97.30	0.00	0.514	0.213	0.273
B11	1024	115.34	95.73	0.01	0.486	0.202	0.297
B12	1122	116.40	97.30	0	0.473	0.197	0.331
B13	1417	116.01	94.12	0	0.445	0.182	0.373
B14	2250	123.36	100.29	0	0.309	0.125	0.566

APPENDIX IV

The bottom and distillate operating temperature, mole fractions of methanol, TMP-1, TMP-2 and TOME of bottoms analysed in third reactive distillation run.

Sample	Time (min)	Bottom T (°C)	Distillate T (°C)	nMEOH	nTMP-1	nTMP-2	nTOME
B1	0			0	0.737	0.256	0.008
B2	90	79	60	0.04	0.740	0.213	0.011
B3	244	80	60	0.04	0.724	0.211	0.028
B4	396	107	79	0.03	0.661	0.221	0.084
B5	456	108	92	0	0.656	0.233	0.111
B6	767	110	87	0	0.621	0.231	0.148
B7	796	111	91	0	0.621	0.231	0.148
B8	882	113	79	0	0.526	0.207	0.267
B9	934	114	94	0	0.499	0.201	0.300
B10	993	114	95	0	0.480	0.196	0.324
B11	1119	116	94	0	0.445	0.182	0.373
B12	1527	116	93	0	0.374	0.152	0.474
B13	1566	122	98	0	0.354	0.145	0.501
B14	1630	122	96	0	0.341	0.140	0.519
B15	1731	122	92	0	0.330	0.134	0.536
B16	1781	123	93	0	0.325	0.131	0.544
B17	1839	123	88	0	0.319	0.128	0.553
B18	1895	124	87	0	0.309	0.125	0.566
B19	1981	125	80	0	0.289	0.111	0.600
B20	2066	127	90	0	0.261	0.102	0.636
B21	2089	128	95	0	0.246	0.098	0.656
B22	2135	128	90	0	0.246	0.097	0.658
B23	2224	129	93	0	0.228	0.090	0.681
B24	2293	129	93	0	0.224	0.088	0.688
B25	2677	128	68	0	0.228	0.084	0.688
B26	2840	129	85	0	0.232	0.084	0.684
B27	2934	130	92	0	0.220	0.080	0.700
B28	2964	130	82	0	0.219	0.080	0.701
B29	3173	130	78	0	0.226	0.082	0.692
B30	3271	130	87	0	0.219	0.080	0.701
B31	3357	131	86	0	0.211	0.078	0.711
B32	3436	131	78	0	0.211	0.079	0.710
B33	3473	132	90	0	0.200	0.076	0.724
B34	3552	130	70	0	0.221	0.081	0.698
B35	3601	107	61	0	0.244	0.085	0.620

APPENDIX V

GC report of the feed utilised for narrow distillation column, after third RD run and distillation.

Peak	RetTime	Width	Area	Height	Area
#	[min]	[min]	[pA*s]	[pA]	%
1	5.01	0.03	442	209	0.263
2	9.44	0.06	62200	15100	36.952
3	9.80	0.05	23300	7342	13.813
4	10.02	0.04	252	99	0.150
5	10.09	0.04	299	115	0.178
6	10.65	0.04	575	246	0.342
7	11.24	0.04	2812	1261	1.670
8	13.00	0.04	344	136	0.205
9	13.92	0.06	78200	16600	46.428

The last bottom sample analysed after the implementation of narrow distillation column to accomplish 99.05 mole percent TOME.

Peak	RetTime	Width	Area	Height	Area
#	[min]	[min]	[pA*s]	[pA]	%
1	11.21	0.04	386	167	0.223
2	12.99	0.06	752	168	0.434
3	13.96	0.08	172000	25900	99.058
4	14.71	0.03	177	97	0.102
5	14.83	0.03	317	139	0.183

APPENDIX VI

The catalytic section (equipped with Amberlyst catalyst) employed for reactive distillation runs.

APPENDIX VII

The measured, literature (Uusi Kyyny et al., 2001) and modelled density, relative and absolute errors for TOME.

T/K	ρ^{meas} (g/cm^3)	ρ^{lit} (g/cm^3)	ρ^{model} (g/cm^3)	Rel. error (%)	Abs. error (g/cm^3)
293.15	0.7986		0.7982	0.0470	0.0004
298.15	0.7946	0.7930	0.7944	0.0302	0.0003
303.15	0.7905		0.7904	0.0067	0.0001
308.15	0.7864		0.7865	-0.0106	-0.0001
313.15	0.7823		0.7825	-0.0212	-0.0002
318.15	0.7782		0.7784	-0.0248	-0.0002
323.15	0.7740		0.7743	-0.0339	-0.0003
328.15	0.7698		0.7701	-0.0351	-0.0003
333.15	0.7656		0.7658	-0.0281	-0.0002
338.15	0.7613		0.7615	-0.0254	-0.0002
343.15	0.7570		0.7571	-0.0134	-0.0001
348.15	0.7526		0.7526	-0.0048	-0.0000
353.15	0.7482		0.7481	0.0144	0.0001
358.15	0.7438		0.7435	0.0448	0.0003
363.15	0.7388		0.7388	0.0055	0.0000
368.15	0.7343		0.7340	0.0487	0.0004
Sum of errors				0.00000078	-0.000013